Development of black ice prediction model using GIS-based multi-sensor model validation

Seok Bum Hong[1], Hong Sik Yun[1,2], Sang Guk Yum[3], Seung Yeop Ryu[4], In Seong Jeong[5], Jisung Kim[3]

[1]Interdisciplinary Program for Crisis, Disaster and Risk Management, Sungkyunkwan University, Suwon, 16419, Korea
5 [2]School of Civil, Architectural Engineering & Landscape Architecture, Sungkyunkwan University, Suwon, 16419, Korea
[3]Department of Civil Engineering, College of Engineering, Gangneung-Wonju National University, Gangneung, 25457, Korea
[4]Disaster Management Office, Korea Expressway Corporation, Gimcheon, 39660, Korea
[5]Disaster and Safety Inspection Division, Disaster Management Cooperation Office, Ministry of the Interior and safety, Sejong, 30116, Korea

10 *Correspondence to*: Jisung Kim (jskim6687@skku.edu)

Abstract. Fog, freezing rain and snow (melt) quickly condense on road surfaces, forming black ice that is difficult to identify and causes major accidents on highways. As a countermeasure to prevent icing car accidents, it is necessary to predict the amount and location of black ice. This study advanced previous models through machine learning and multi-sensor verified results. Using spatial (hill shade, slope, river system, bridge, and highway) and meteorological (air temperature, cloudiness,
15 vapour pressure, wind speed, precipitation, snow cover, specific heat, latent heat, and solar radiation energy) data from the study area (Suncheon-Wanju Highway in Gurye-gun, Jeollanam-do, South Korea), the amount and location of black ice were modelled based on system dynamics to predict black ice and then simulated with Geo-Information System in units of 1 m^2. The intermediate factors calculated as input factors were road temperature and road moisture, modelled using a deep neural network (DNN) and numerical methods. Considering the results of the DNN, the root mean square error was improved by
20 148.6% and reliability by 11.43% compared to a previous study (Linear Regression). Based on the model results, multiple sensors were buried at four selected points in the study area. The model was compared with sensor data and verified with the upper-tailed test (with a significance level of 0.05) and Fast Fourier Transform (freezing does not occur when wavelength = 0.00001 Hz). Results of the verified simulation can provide valuable data for government agencies like road traffic authorities to prevent traffic accidents caused by black ice.

1 Introduction

25 Meteorological conditions such as fog, freezing rain, and snow lead to the formation of black ice in dark and cold places, such as bridges, tunnel entrances, and shady roads. Black ice is a thin coat of ice on black asphalt, making it difficult for drivers to visually distinguish it from public roads (Cary, 2010). Black ice can cause significant traffic accidents because it occurs rapidly in weather conditions such as freezing rain (Kämäräinen et al., 2017). Over the past five years, the number of fatalities in traffic accidents due to black ice is four times that of fatalities caused by snow (Kim, 2021b). In winter, the fatality rate is
30 higher than that of general road conditions otherwise. Therefore, it is essential to implement measures to prevent traffic

accidents. Research is needed to predict and verify the amount and location of black ice using modelling as a basis for establishing countermeasures.

35   This study predicted the amount and location of black ice by modelling winter ice on a Korean mountainous highway in winter and simulated using the Geographic Information System (GIS). Subsequently, the model was verified using a multi-sensor. Korea has four distinct seasons, and in winter, the temperature drops to a minimum of $-10°C$ (An and Choi, 2013). In addition, Korea is surrounded by sea on three sides, and various types of inland water bodies such as lakes, rivers and mountainous regions are evenly distributed; thus facilitating formation of black ice (Cary, 2010). Various types of icing traffic accidents occur annually, depending on the environment prone to black ice (Authority, 2017). On 3 December 2021, nine ice

40   accidents occurred in Chungbuk, Korea, from 5 am to 11 am. At 7:38 am, seven vehicles collided on the road in Saenggeuk-myeon, Eumseong-gun, and Chungcheongbuk-do, injuring two people. At 8:30 pm, 1-ton trucks hit each other in Chilseong-myeon, Goesan-gun, and Chungcheongbuk-do, and one person was injured (Yunhap, 2021). On the morning of 6 January 2020, 41 vehicles collided on National Highway 33 in Gyeongsangnam-do, wounding ten people (Lee, 2020). On 14 December 2019, a chain collision occurred on the Sangju-Yeongcheon Highway due to black ice, killing seven people and injuring 42

45   others (Jung, 2019). On the morning of 15 November 2019, black ice caused a chain collision of 20 vehicles, resulting in significant damage (Kim, 2019). Analysis of these cases revealed an average of $-1.9°C$ to be the lowest temperature on the days of the incidents, and the average cloud cover was 5.6 (maximum 10). The average daily precipitation was 4.3 mm, and the average sunrise time was 07:28 am. The average accident time was 07:05 am (Kma, 2018). Traffic accidents usually occur in the morning around the time of sunrise when there is precipitation on average and the minimum temperature is below $0°C$.

50   Various studies have been conducted on black ice, and the cause of its occurrence has been elucidated to some extent. There are multiple causes, such as freezing of moisture formed due to fog on road surfaces, rain water from during the day that is subsequently frozen at night, rapid freezing of freezing rain, and re-freezing of melted snow (Cary, 2010). Among them, the cause of high fatality is "Freezing Rain", i.e. extremely cooled rain that does not have enough time to freeze below 0 °C before it hits the ground/road surface, and then freezes rapidly at the moment of impact (Cheng et al., 2007). As freezing rain freezes

55   as soon as it hits the road, it is difficult to intuitively predict the amount and location of black ice (Hull, 1999). Therefore, it is essential to select a vulnerable section where black ice is expected based on fog (moisture), freezing rain, and snow (melt), and prevent icing traffic accidents through structural or non-structural measures.

Modelling the amount and location of black ice and a GIS simulation process based on this are required to select sections vulnerable to freezing traffic accidents. Black ice modelling for GIS simulation was performed based on system dynamics, a

60   method of simulating dynamic phenomena by connecting the causal relationships of factors in the form of a block diagram (Kim, 2021a; Forrester, 1994). Road freezing is difficult to predict with human intuition, as it occurs due to the time-series relationship of factors; thus, system dynamics are more suitable for modelling this phenomenon (Terzi et al., 2021b). GIS is a tool for simulating system dynamics and conducting research on various disasters. Studies using GIS include: ice and snow analysis (Jeong et al., 2019; Koumoutsaris, 2019; Bardou and Delaloye, 2004; Cheng et al., 2007), flood analysis (Wang et al.,

65 2021), underwater volcanic eruption modelling (Hayward et al., 2022), traffic analysis during natural disasters (Toma-Danila et al., 2020), earthquake and landslide analysis (Yi et al., 2019; Ali et al., 2019), among others. In this study, as well as in predicting and mapping (simulation) black ice, GIS was applied by referring to previous disaster-related studies. The GIS-System dynamics modelling study was based on spatial and meteorological data. In this study, we used digital elevation model, hill shade, road, bridge, river system, and lake as spatial data and air temperature, cloudy, vapor pressure, precipitation, wind

70 speed, snow (melted), specific heat, latent heat, and solar radiation energy as meteorological data. Prior to starting a full-scale study using major factors, previous studies on related topics were analysed to explore the justification of black ice modelling and validation studies. The representative studies are as follows.

Kangas et al. performed numerical modelling of factors related to black ice. They predicted road surface conditions and traffic conditions using the NWP model. However, the prediction of the location and the generated amount of road icing is

75 insufficient, and the model lacks validation (Kangas et al., 2015).

Bezrukova et al. performed numerical modelling to predict the occurrence of black ice. They developed a block diagram model to estimate the ice index based on road surface temperature, air temperature, and humidity. Their model could predict the occurrence of black ice at a superficial level. However, the prediction of the location and amount of black ice was insufficient, and the model was not validated. (Bezrukova et al., 2006)

80 Chapman et al. estimated road temperature through numerical modelling. They analysed the relationship between road temperature and latitude, altitude, sky-view factor, screening, roughness length, road construction, traffic density, and topography. However, the prediction of the amount and location of black ice is insufficient and the model was not validated (Chapman et al., 2001).

Lee et al. performed numerical modelling related to the black ice on the Jeju Island, the southernmost island in Korea.

85 Although the air temperature and wind speed were predicted using the WRF model, the prediction of road icing was insufficient, and the model was not validated (Lee et al., 2018).

Hong et al. estimated the amount and location of black ice based on system dynamics and simulated the results using GIS. The linear regression analysis, the most basic statistical analysis technique, was used for road temperature prediction, and black ice-related factors are relatively simple. However, the black ice prediction model has not yet been validated (Hong et al.,

90 2021).

Liu et al. proposed sensor-based GIS visualisation technology for black ice management. The traffic danger section was visualised by interpolating sensor information using overlapping spatial data, such as roads, on the GIS. In addition, a methodology for determining whether black ice is generated by the fusion of an ice sensor based on electrical conductivity and temperature information has been presented. Although the sensor monitoring technique has been efficiently proposed, the

95 modelling part is insufficient, and the sensor configuration is simple (Liu et al., 2017).

In another study, simple numerical modelling was used to predict Black Ice. Related studies include road temperature prediction using the integrated model of the Korea Meteorological Administration (KMA) (Park et al., 2014), heat conduction analysis due to air temperature and humidity of road surface (Sass, 1992), salinity and temperature measurement and analysis

of road surface (Xu et al., 2017) , and development of black ice estimation algorithm for sensors (Troiano et al., 2010; Teke
100   and Duran, 2019). As in previous studies, the estimation of the amount and location of black ice was insufficient, and there
was no model validation.

Using these methods, factors related to black ice can be systematically predicted. However, in many studies, the combination
of spatial and meteorological data is insufficient, and the simulation step for the location of occurrence has been omitted. In
addition, most studies have not performed model validation using sensors. Incorporating the amount and location prediction
105   step in the numerical modelling of black ice improves its efficiency and aids in preparing for traffic accidents in winter, going
beyond simple road temperature prediction (Chapman et al., 2001). A previous, study system dynamics modelling for
estimating the locations of road icing using GIS, by Hong et al. predicted the occurrence and location of Black Ice (Road Icing)
using both meteorological and spatial data, which was simulated using GIS (Hong et al., 2021). However, because the previous
study predicted road temperature, the most critical factor in black ice prediction, using a relatively simple statistical analysis
110   technique of linear regression, it is necessary to improve the prediction accuracy using a more advanced technique. In addition,
consideration of black ice-related factors, such as specific heat, latent heat, solar radiation energy (per hour), and snow (melt),
is insufficient, and additional modelling of these factors is required (Liu et al., 2021). Moreover, as in other cases, the validation
of the model is insufficient. Compared with previous studies (Hong et al., 2021), the areas developed in this study are shown
in Table 1. In this study, Gurye, Jeollanam-do, with a more significant proportion of mountainous regions than Suncheon,
115   Jeollanam-do, was selected as the study area. The added factors are specific heat, latent heat, solar radiation energy (per hour),
snow (melting), etc. Through the added factors, the phenomenon of water generation at temperatures above 0°C after snowfall
and the phenomenon of black ice melting by the sun's heat were realised through system dynamics. As mentioned above, road
temperature was predicted among the model components through linear regression analysis. The model was improved by
combining a deep neural network and an evolution algorithm to develop it from a simple method further. Subsequently, the
120   validity was verified by installing a multi-sensor at the predicted location of the black ice. This study aimed to develop a
complete black ice model by improving the modelling of previous studies and verifying the model using sensor technology. A
reliable black-ice simulation derived using a verified model can be used by government agencies (e.g. road traffic authorities)
to identify areas vulnerable to winter traffic accidents in advance and prevent them.

Table 1: Developments of this study compared to previous studies.

	Study Area	**Factors (added)**	**Model (Road Temp)**	**Result**	**Validation**
Previous Study (Hong et al., 2021)	Suncheon, Jeollanam-do, South Korea	-	Linear Regression Model, Evolution Algorithm (Train Set: 98)	Amount and location of Black Ice (GIS)	-

Current Study	Gurye, Jeollanam-do, South Korea	Specific Heat, Latent Heat, Solar Radiation (per Hour), Snow (Melted Amount)	Deep Neural Network Model, Evolution Algorithm (Train Set: 1498)	Amount and location of Black Ice (GIS)	Multi-sensor and comparison analysis

2 Methodology

As shown in Figure 1, the research was primarily composed of three stages. The first step was to establish the research methodology corresponding to Phase 2, which defined the study area, data, and algorithm. The second step, which corresponded to Phase 3, defined a scenario and derived modelling results. The road temperature and road moisture were calculated using system dynamics, and the amount and location of black ice were predicted. The third step, which corresponded to Phase 4, verified the model using a sensor. For the validation of the model, a hypothesis test (Z-test, one-tailed test) was performed with a significance level of 0.05 for the section predicted by the model for the round force value, which was the core data. For the remaining data (water pressure, ultrasonic, temperature, and humidity), the model's validity was verified through fast Fourier transform, Z-test, and graph comparison methods.

2.1 Model flow and data definition

This study attempted to model and simulate the occurrence of black ice, for which appropriate data selection was required. Before collecting the actual data, the data type and format were selected, and a system dynamics model that could handle the causal relationship between data (factors) was constructed. Powersim Studio version 10.0 was used as the software for operating the system dynamics method (Kim, 2021a). A schematic of the system dynamics model designed in Powersim is shown in Figure 2, which shows a causal map of the system dynamics structure. The causal map expresses the causal relationship of dynamic variables and directly describes the operating procedure of system dynamics (Kim, 2021a; Forrester, 1994).

The +/– signs in the causal map express causal relationships between the variables. In the case of +, the before and after factors are proportional and inversely proportional, respectively. In the causal map, B represents a balanced loop and maintains the total amount of a specific state. In the model used in this study, the relationship between road moisture and freezing corresponded to a balanced loop. In the final stage, freezing and black ice have a positive relationship, and thawing and black ice have a negative relationship (Sterman, 2000; Terzi et al., 2021a). In other words, freezing and thawing per hour are determined by several factors, and the amount of black ice generated per hour is predicted accordingly. A system dynamics block diagram, which is the basis of the causal map in Figure 2, is shown in Figure A1.
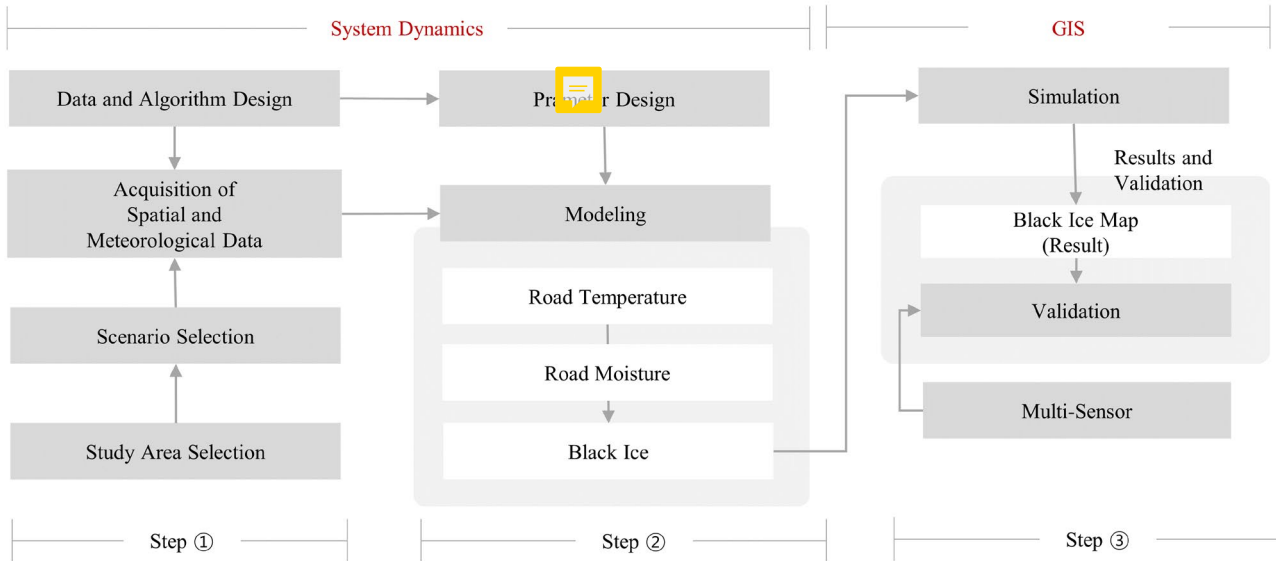
150 **Figure 1:** Summary of black ice modelling and sensor validation studies.

In the system dynamics model, spatial data are hill shade (from DEM), road, bridge, river system, and lake, and weather data are air temperature, cloudy, vapour pressure, precipitation, wind speed, snow (melted), specific heat, latent heat, and solar radiation energy. The system dynamics used in black ice modelling lists the elements that cause specific phenomena on a block diagram and shows their relationships over time. When spatial and meteorological data are entered into the system dynamics,

155 they are calculated sequentially according to the causal relationship of the elements, and the output, black ice, is calculated through the intermediate factor. The intermediate factors, road temperature and road moisture, were calculated each time by reflecting the dynamic characteristics of the inputs. Road temperature is expressed as a function of hill shade, bridge, air temperature, and cloud cover, and road moisture is defined as a function of vapour pressure, precipitation, snow (melt), and wind speed. Black ice was predicted per hour according to the dynamic characteristics of the two intermediate factors. The

160 expected amount and location of black ice generation were simulated using GIS in units of 1 m^2. Table 2 lists the required parameters. The model definition expressing the relational expressions between the significant factors is shown in Table A2.

Table 2: Main input and output factors of the model.

Factor	Category	Symbol	Value Range	Unit
Hill shade (From DEM)	Spatial	H	0~254	-
Bridge Location	Input	L_b	0 or 1	-
River System	(t = 0–13 hour)	RS	0~1	-
Lake		L	0~1	-
Air Temp	Meteorological	T_a	−15~10	°C
Cloudy		V_c	0~10	-

Vapour Pressure	Input	P_v	0 or more	Pa
Precipitation	(t = 0–13 hour)	Pr	0 or more	mm
Wind Speed		S_w	0 or more	m/s
Snow (Melted)		S_m	0 or more	mm
Specific Heat		H_s	0 or more	Cal/g°C
Latent Heat		H_l	0 or more	Cal/g°C
Solar Radiation Energy		E_{sr}	0 or more	Cal
Evaporation	Intermediate	E	0 or more	g/m³
Condensation	(t = 0–13 hour)	C	0 or more	g/m³
Road Temperature	Output	Tr	−15~10	°C
Road Moisture		Mr	0 or more	g/m³
Black Ice	(t = 0–13 hour)	BI	0 or more	g/m³

165
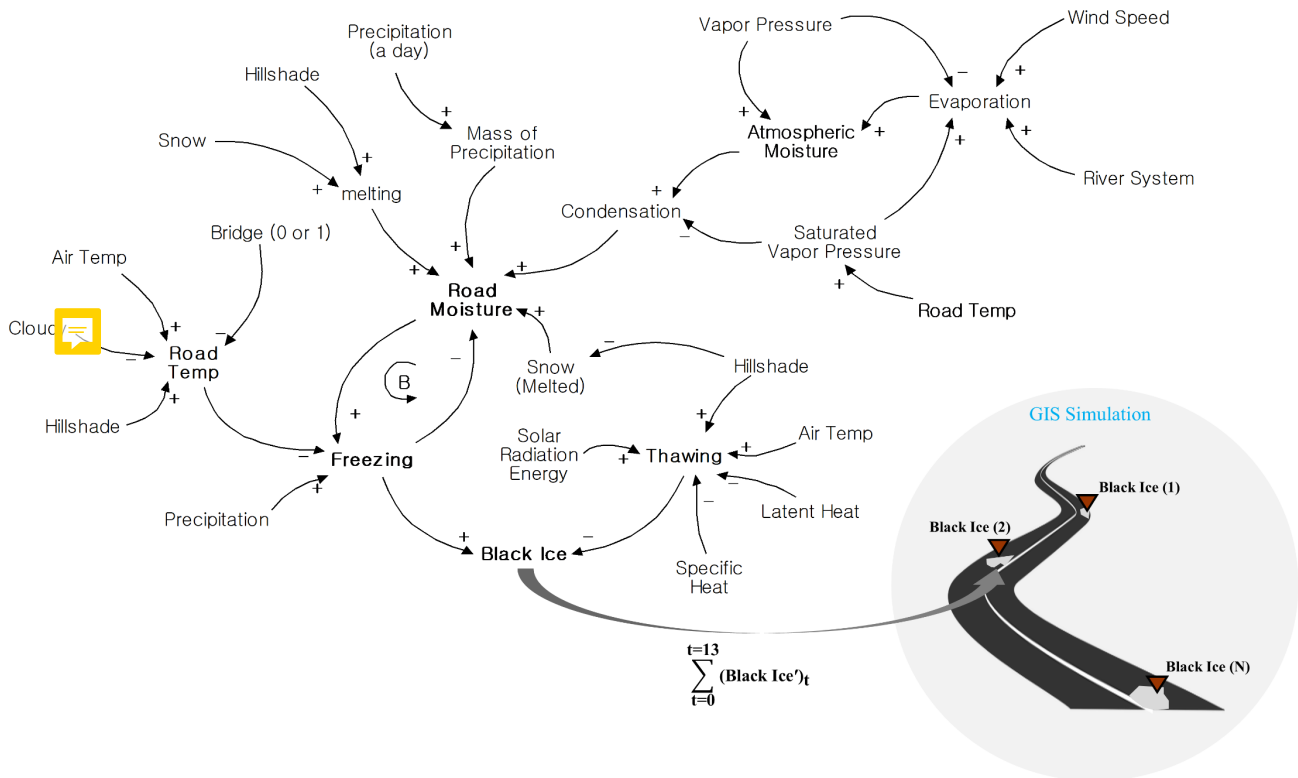
Figure 2: Causal loop of system dynamics model. A causal loop is constructed according to the causal relationship of each factor, and the main results are Road Temperature, Road Moisture, and Black Ice. [+] means proportional, and [–] means inverse proportion.

2.2 Road temperature and moisture modelling

170

Road temperature and road moisture are important intermediate factors in the generation of black ice and were calculated as input data. These two factors are essential because freezing water on the road surface at sub-zero temperatures is the basic principle of black ice formation (Cary, 2010). The road temperature should be appropriately predicted to determine the formation of black ice. The existing prediction method required weather variables, such as solar radiation energy, air

175 temperature, atmospheric pressure, wind, and thermal characteristic values according to the road surface material (Park et al., 2014). However, this method requires many factors when predicting road temperature, and calculation errors can easily occur because of missing data. Given the nature of the simulation, which requires high efficiency and limited data, this area needs to be improved. In this study, we devised a method that can produce high prediction performance with a small number of input factors through the combination of a deep neural network (DNN) and an evolution algorithm (Peng et al., 2022).

180 The factors entered into the deep neural network model were hill shade (H), air temperature (Ta), and cloudy (C). Each factor is entered into the system dynamics by the following stock-flow model: variables (V_{RT}) related to road temperature were entered using Eq. (1). The above-mentioned H, L_b, T_a, and C can be substituted for the variable V_{RT}, which is calculated by adding the integral value according to time (t = 0 to 13) to the initial value (t = 0).

$$V_{RT} = \int (V_{RT}')_t + (V_{RT})_{t=0} , \tag{1}$$

185 The road temperature can be directly predicted using the in-variable of Eq. (1). Previous studies have used a linear regression model and evolution algorithm for road temperature prediction (Hong et al., 2021). The linear regression model parameters were trained using 98 datasets, including H, L_b, T_a, and C. However, when the amount of data increases, the prediction ability becomes relatively low, and this method is not robust with various types of cases. In this study, 1498 data sets were obtained for H, L_b, T_a, C, and a DNN model was introduced to predict road temperature in various weather conditions

190 such as fog, rain, and snow. The structure of the DNN implemented in system dynamics is shown in Figure 3. The DNN consists of three hidden layers: the first layer has three neurones, while the second and third layers have four neurones, and each neuron has weight and bias. Equation 2 is a linear function with a weight (Wn) and bias (Bn). Equation 3 is an activation function corresponding to the ReLU function. The ReLU function returns 0 when the input x value (lf) is less than 0 and returns the value as it is when x value is greater than 0. As the maximum value can be greater than one when ReLU is used, vanishing

195 gradients can be prevented, and the learning speed is faster (Kelleher, 2019).

$$lf = \sum_1^n (x \cdot w_n) + b_n , \tag{2}$$

$$af = \begin{cases} lf, & lf > 0 \\ 0, & lf \le 0 \end{cases}, \tag{3}$$

The DNN block diagram of the system dynamics and schematic diagram of the evolution algorithm are shown in Figure 3. Parameter (Wn, Bn) optimisation of the DNN model was performed using the evolution algorithm. The deep learning method

200 based on the existing gradient descent and back propagation is quicker by dynamic programming but it is not suitable for

application to the system dynamics environment with dynamic characteristics owing to the time change (Mitra et al., 2021). Therefore, the parameters of the DNN are optimised with the evolution algorithm, which is versatile for models with various characteristics such as dynamic change. Among the processes of the evolution algorithm, encoding involves changing the parameters of the model to be optimised into the genetic form of the evolution algorithm. If several candidates are generated

205 by encoding, fitness is evaluated using a fitness function. The fitness function is given by Eq. (4). This is the mean absolute percentage error function between the actual and predicted values, and the termination condition is when it is minimum (De Myttenaere et al., 2016). When the parent solution is updated with solutions whose fitness is highly evaluated by the fitness function, the parent solutions are transferred to the genetic operator process to perform crossover and mutation. The child solutions created in the genetic operator process return to the fitness measure process and the termination condition is evaluated.

210 If the termination condition is not satisfied, the genetic operator is repeated, and the solution gradually converges. As the solution converged, the error between the predicted road temperature and the actual road temperature changed to the minimum value. A MAPE value of 20% or less implied appropriate prediction (reliability of 80% or more) (Holland, 1984).

$$F(t) = \frac{100\%}{n} \sum_{t=0}^{t=13} \left| \frac{A_t - F_t}{A_t} \right|, \tag{4}$$

It is known that the temperature on bridges is 1–2°C lower than that on general roads (Tabatabai and Aljuboori, 2017;

215 Rathke and Mcpherson, 2006). Accordingly, we performed a temperature correction on the road passing through the bridge based on the road-temperature prediction value. In Eq. (5), T_r is the road temperature and Time is the time in the simulation (~ 0–13 h). Subsequently, reliability was used to evaluate the accuracy of the simulation train and test. Reliability is obtained by converting the F(t) value (MAPE) into a percentage and subtracting it from 100%.

$$T_r = T_r(-1 - \frac{Time}{13}), \tag{5}$$

220 $$MAPE = \frac{100\%}{n} \sum_{t=0}^{t=13} \left| \frac{T_r - F_t}{T_r} \right|, \tag{6}$$

$$Reliability = \{1 - MAPE\} * 100 (\%), \tag{7}$$

Road moisture must also be appropriately predicted to judge the formation of black ice. When moisture is formed on the road, it becomes possible to judge the generation of black ice over time with the dynamic characteristics of road temperature. There are three typical cases of moisture generation that cause black ice on roads (Zerr, 1997).

225 Case (1): Water vapour condenses on the road when the road temperature drops below the dew point.

Case (2): Freezing rainfalls at below 0 °C road temperature.

Case (3): Water formation when the accumulated snow melts due to sun's heat.

Factors related to road moisture include vapour pressure, precipitation, wind speed, snow (melted), specific heat, latent heat, and solar radiation energy. The stock-flow model inputs vapour pressure, precipitation, wind speed, and snow (melted), such

230 as road temperature factors, and their contents are the same as those in Eq. (8). The aforementioned P_v, P_r, S_w, and S_m can be

substituted for the variable V $_{RM}$, which is calculated by adding the integral value according to time (t = 0–13) to the initial value (t = 0).

$$V_{RM} = \int (V_{RM}')_t + (V_{RM})_{t=0} \, , \tag{8}$$
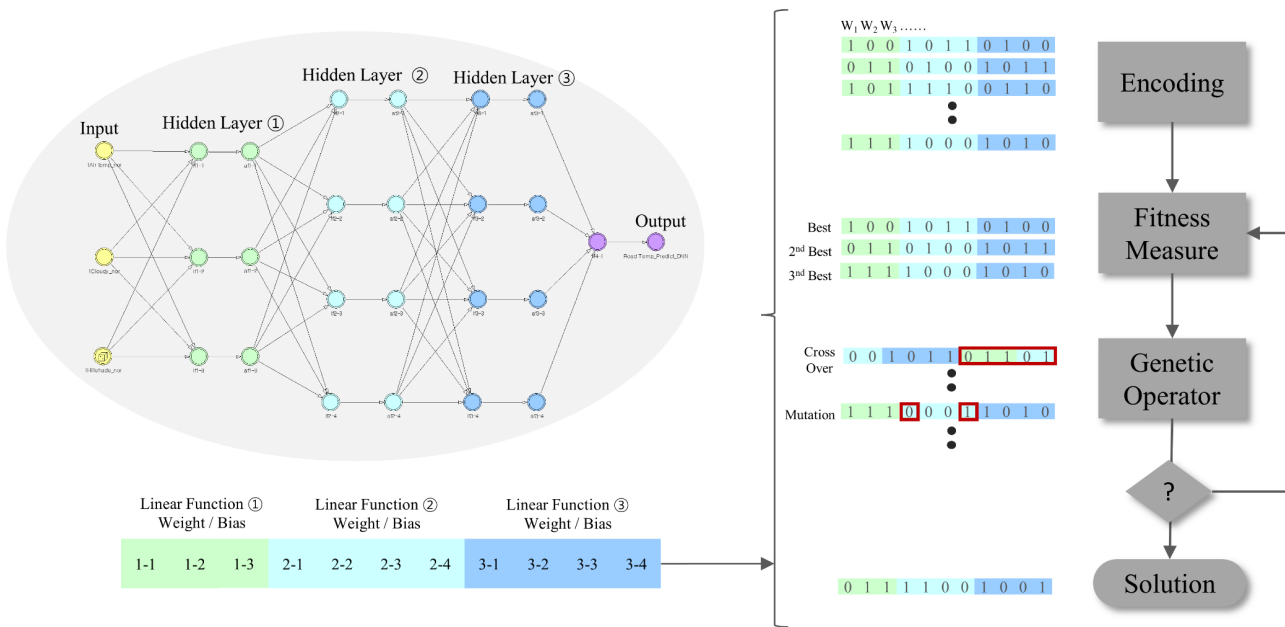
Figure 3: Structure of system dynamics of deep neural network for Road temperature modelling. (a) Change the parameters of DNN in the form of the chromosome. (b) The fitness function of the chromosome is evaluated and input to the Genetic operator. (c) It performs selection to select chromosomes with high fitness, crossover to mix gene values, and mutations to simulate mutations in gene values. (d) Choose a solution based on the goodness of fit

The formula for road moisture (Mr) using condensation, mass of precipitation, snow (melt) is as follows in Eq. (9). The mass of precipitation (MoP) is the mass of precipitation (g/m^3) and C is the condensation (g/m^3). If black ice occurs at freezing, road moisture is reduced.

$$M_r = \sum_{t=0}^{t=13}(MoP + C - F \ldots \tag{9}$$

Precipitation and mass of precipitation are weather-related factors on rainy days, as shown in Figure 2. The MoP in Eq. (9) represents the actual mass of precipitation per hour in 1 m^3. In Eq. (10), P is the amount of precipitation (mm) converted to centimetres when the mass was calculated.

$$MoP(g/m^3) = \frac{\pi r^2 P}{10} \tag{10}$$

The condensation (C) in Eq. (9) is calculated using the equation between the amount of water vapour present in the atmosphere and the amount of saturated water vapour on the road. Condensation occurs when the temperature of water vapour in the atmosphere drops below the dew point on the road surface. The condensation contents are given by Eq. (11), where E is the evaporation (g/m3), V is the amount of vapour (g/m3), and V_s is the amount of saturated water vapour (g/m3).

$$C = \sum_{t=0}^{t=13}(E + V - V_s) , \tag{11}$$

The evaporation (E) in Eq. (11) is based on aerodynamics, and Dalton's law describing evaporation. Dalton's law states that the movement of water molecules on a free surface is proportional to the vapour pressure gradient in the vertical direction. The formula for this theory is given by Eq. (12), where E is the amount of evaporation from the reservoir, e_s is the saturated water vapour pressure at air temperature(mmHg), P_v is the actual vapour pressure at air temperature (mmHg), and S_w is the wind speed (m/s) at a height of 2 m from the water surface (Silberberg, 2009).

$$E = 0.345(e_s - P_v)(0.5 + 0.54S_w) , \tag{12}$$

The amount of vapour (V) in Eq. (11) can be obtained using Eq. (13), where P_v is the vapour pressure and T_a is the temperature of the air.

$$V = 217\frac{P_v}{T_a+273.15} \tag{13}$$

2.3 Black Ice Modelling and Simulation

The amount and location of black ice generation per hour can be predicted by calculating the road temperature and road moisture. The black ice model is an integral value for the change in freezing and thawing (Pradhan et al., 2019). Equation 14 is as follows:

$$BI = \int(F - Th)_t' dt \tag{14}$$

Freezing is a function of the road temperature (Tr), road moisture (Mr), and precipitation (P). In the presence of road moisture, freezing changes when the road temperature reaches a specific condition. If the precipitation is greater than zero, freezing occurs when the road temperature is less than 1°C. If the precipitation is 0, freezing occurs when the temperature is below 0°C (Bonanno et al., 2010). The contents are the same as those in Eq. (15).

$$F_t' = f(T_r, M_r, P) = \begin{cases} M_r \ (P > 0 \ and \ T_r < 1) \\ M_r \ (P = 0 \ and \ T_r < 0) \end{cases} \tag{15}$$

Thawing is a function of black ice (BI), hill shade (H), air temperature (T_a), specific heat (H_s), latent heat (H_l), and solar radiation energy (E_{sr}). The amount of energy required for thawing (H_n) was calculated as the sum of latent heat and specific heat (Pradhan et al., 2019). The air temperature is above or below zero acts as a condition for thawing.

$$H_n = H_s * BI * \Delta T_r + H_l * BI * \Delta T_r \tag{16}$$

$$Th_t' = \begin{cases} \frac{\left(\frac{H}{250}\right)E_{sr}}{H_n} BI \ (T_a > 0) \\ 0 \ (T_a < 0) \end{cases} \tag{17}$$

As shown in Figure 2, the predicted amount and location of black ice per hour were simulated in 1 m² units using GIS. Black ice was modelled from 00:00 AM to 13:00 PM, the time range where the occurrence and traffic accidents were most frequent, and the total amount of black ice generated at all times was simulated in GIS.

280 $$BI_{t=0..13} = \sum_{t=0}^{t=13} BI_t \tag{18}$$

3 Results (application of black ice scenario)

3.1 Black ice scenario

Gurye-gun, Jeollanam-do, Korea, was used as the study area, which is adjacent to the southern coast, and the water system and mountainous regions are evenly distributed inland. The highway in this area is prone to moisture and shade; as a result, it

285 was expected to be prone to black ice (Shao and Lister, 1995). As shown in Figure 4, the maximum elevation of Gurye-gun and Jeollanam-do is 1731 m (Esri). The average elevation is 420.4 m, which corresponds to the representative mountainous region of Jeollanam-do. Jirisan, which belongs to Gurye-gun, is the highest mountain in Jeollanam-do, with a maximum elevation of 1916.77 m (Wikipedia, 2022). The Suncheon Wanju Highway in Gurye-gun, which is ~ 16 km (Figure 4 A–B), passes through the water system and mountainous areas on the left and right [Figure 4 (a)–(b)], which is an environment prone

290 to black ice. In addition, there are ten bridges in the 16 km section. Bridges have an average temperature of 1–2°C lower than that of general roads; therefore, black ice is more likely to occur even at the same temperature (Tabatabai and Aljuboori, 2017; Xue et al., 2018). Therefore, Gurye-gun in Jeollanam-do, an area vulnerable to black ice, was selected as the black ice research area, and data collection and modelling were performed.

Actual days of black ice were selected as scenarios to verify the validity of the previously designed model. Data were

295 acquired between December 16–19, 2021, by installing a multi-sensor that can detect black ice on a parted section of the Suncheon-Wanju Highway located in Gurye-gun, Jeollanam-do, South Korea. For this period, all three cases of fog (moisture), freezing rain, and snow (melted) could be confirmed; therefore, it was selected as a study scenario. The average values of the weather information for the relevant days are listed in Table 3. On 16 December, the maximum value of humidity was 100%, and the temperature was a minimum of 0.3 °C; hence, it was analysed that fog had caused the freezing.
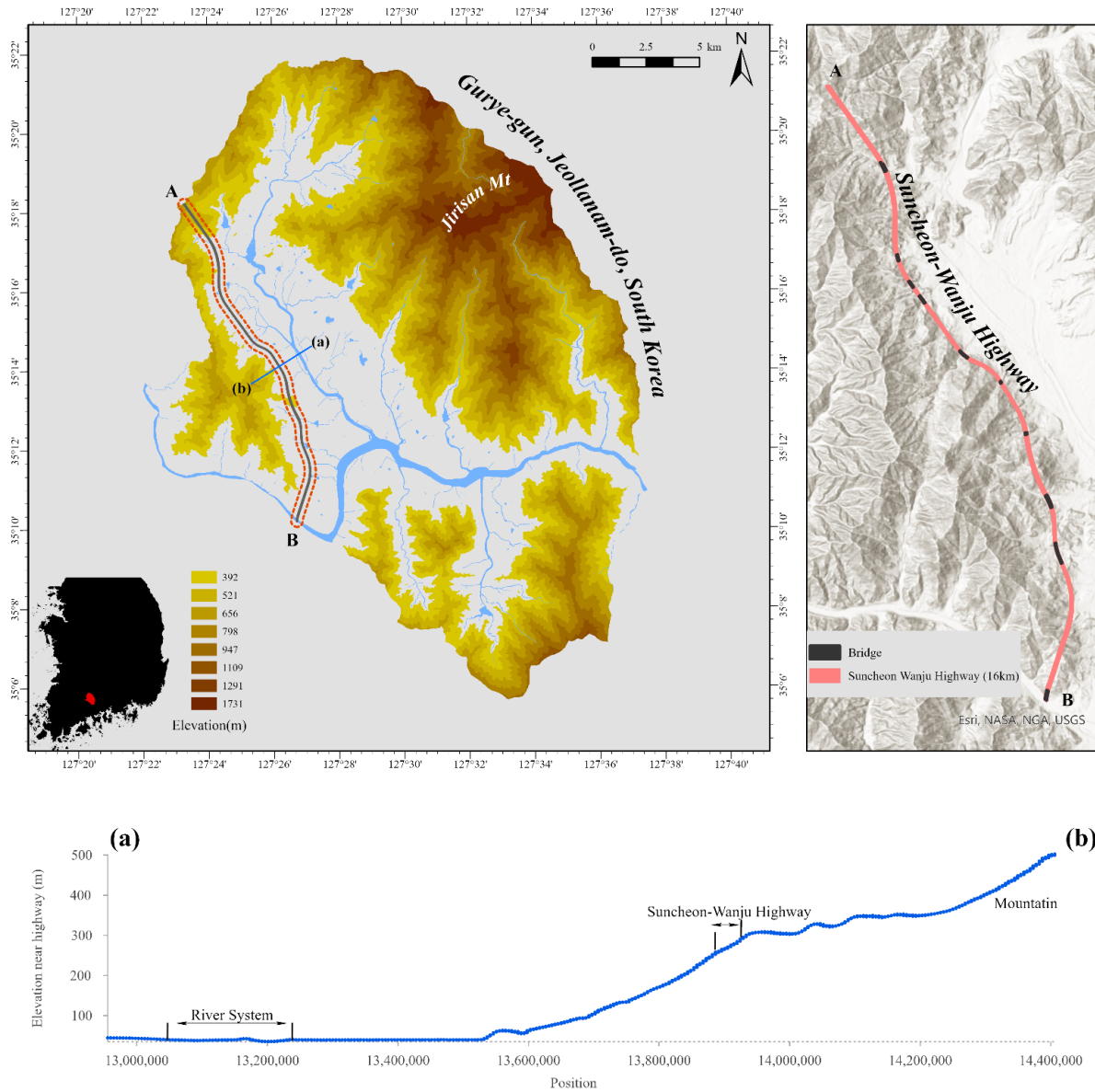
Figure 4: Suncheon-Wanju highway, Gurye-gun, Jeollanam-do, a research area for system dynamics model. The Suncheon-Wanju Expressway in Gurye-gun, Jeollanam-do runs from point A (35°18'S) to point B (35°10'S). If the section from (a) to (b) is selected and the cross-section is analysed, mountains and water systems are observed to the left and right.

On December 17, precipitation and temperature dropped below zero and coinc[de], the precipitation amount was 0.7 mm, and the lowest temperature was –4.1°C, which was analysed to be freezing rain. It was interpreted that there was snow cover on December 18–19, and there was a time when the air and ground temperature was 0 °C or higher. Hence, the snow melted, and the phenomenon of freezing occurred again (Kma, 2018). Therefore, 16 December was set as the fog scenario, 17 December as the freezing rain scenario, and December 18th and 19th as the snow scenario in this model.

310 **Table 3:** A list of scenarios for the system dynamics model. Validate the model by acquiring sensor data from the dates in the list.

Date	Air Temp (Av/Min, °C)	Precipitation (a day, mm)	Humidity (Ave/Max, %)	Snow Cover (Ave/Max, cm)	Ground Temp (Av/Min, °C)	Type
2021/12/16	5.2/–0.3	2.1	90/100	0/0	5.2/0.1	Fog
2021/12/17	1.6/–4.1	0.7	78/95	0/0	1.7/0.3	Freezing Rain
2021/12/18	–2.1/–7.2	0	62/87	1.1/1.6	1/–0.5	Snow
2021/12/19	1.2/–3.2	0	76/96	0.3/0.4	1.2/–1.9	Snow

After establishing the scenario, the spatial and meteorological data for the selected date were entered into the model. Spatial data were obtained from the Lidar satellite, National Spatial Data Infrastructure Portal (NSDIP), etc. Meteorological data were obtained from automatic weather stations (AWS) and an automated surface observing system (ASOS) operated by the Korea

315 Meteorological Administration (Kma, 2018). The DEM had a resolution of 5 m and was interpolated to 1 m to produce the hill shade data. Bridges, roads, river systems, and lakes were converted into 1 m resolution raster information. The AWS, which acquired weather data, is located in Gurye and provides air temperature, wind speed, and precipitation data. However, with AWS, the types of data that can be acquired are limited, so the remaining meteorological data were obtained from the ASOS in Suncheon, a nearby city. The data received from the ASOS were cloudy, vapour pressure, and snow (melt). Specific heat,

320 latent heat, and solar radiation energy were entered directly into the system dynamics without linking with the GIS. By obtaining the scientific experimental values through literature research, we can calculate the size of each point using the mass of ice and hill shade. The results are listed in Table 4. Hill shade and meteorological input data were from the period between 00:00 AM to 13:00 PM. As mentioned in the Introduction section, most black ice traffic accidents occurred from dawn to morning, and the average temperature reached its peak at 13:00. For the efficiency of the simulation, the time range was set

325 from early morning to 13:00 PM when the amount of air temperature and solar radiation energy was low, but the traffic volume was high.

Table 4: Factor list and data information of system dynamics model.

Factor	Category	Data Source	Resolution	Time Range	Content
Hill shade (From DEM)	Spatial Input	Lidar Satellite (5 m)	1 m (Interpolation)	AM 00:00 –PM 13:00	Scenario Input Train Set
Bridge Location		NSDIP	1 m	-	Scenario Input
River System		NSDIP	1 m	-	Scenario Input
Lake		NSDIP	1 m	-	Scenario Input
Air Temp	Meteorological	AWS	1 m	AM 00:00 –PM 13:00	Scenario Input Train Set

	Input				
Cloudy		ASOS	1 m	AM 00:00 –PM 13:00	Scenario Input Train Set
Vapour Pressure		ASOS	1 m	AM 00:00 –PM 13:00	Scenario Input
Precipitation		AWS	1 m	AM 00:00 –PM 13:00	Scenario Input
Wind Speed		AWS	1 m	AM 00:00 –PM 13:00	Scenario Input
Snow (Melted)		ASOS	1 m	AM 00:00 –PM 13:00	Scenario Input
Specific Heat		literature	1 m	AM 00:00 –PM 13:00	Scenario Input
Latent Heat		literature	1 m	AM 00:00 –PM 13:00	Scenario Input
Solar Radiation Energy		literature	1 m	AM 00:00 –PM 13:00	Scenario Input

3.2 Black ice system dynamics modelling results

330   A DNN model was introduced to model road temperature, and an evolution algorithm was used for parameter optimisation. A total of 1498 training sets were used for parameter optimisation (weight and bias), and each consisted of hill shade, air temperature, and cloudy conditions. The training reliability obtained using the training set is shown in Figure 5. Figure 5 (a) and (b) show the training result reliability of the DNN and linear regression (LR), respectively. The reliability of the graph was recorded at time 13. Previous studies used the LR model for road temperature prediction (Hong et al., 2021). The training

335   reliability of the model of the previous study (RL) and that of the current study (DNN) was compared. The results were 93.01% for DNN and 91.4% for LR. In addition, when the root mean square error (RMSE) was applied as another error index, the DNN was 1.6 and LR was 1.67. That is, the training performance of the DNN was found to be better.
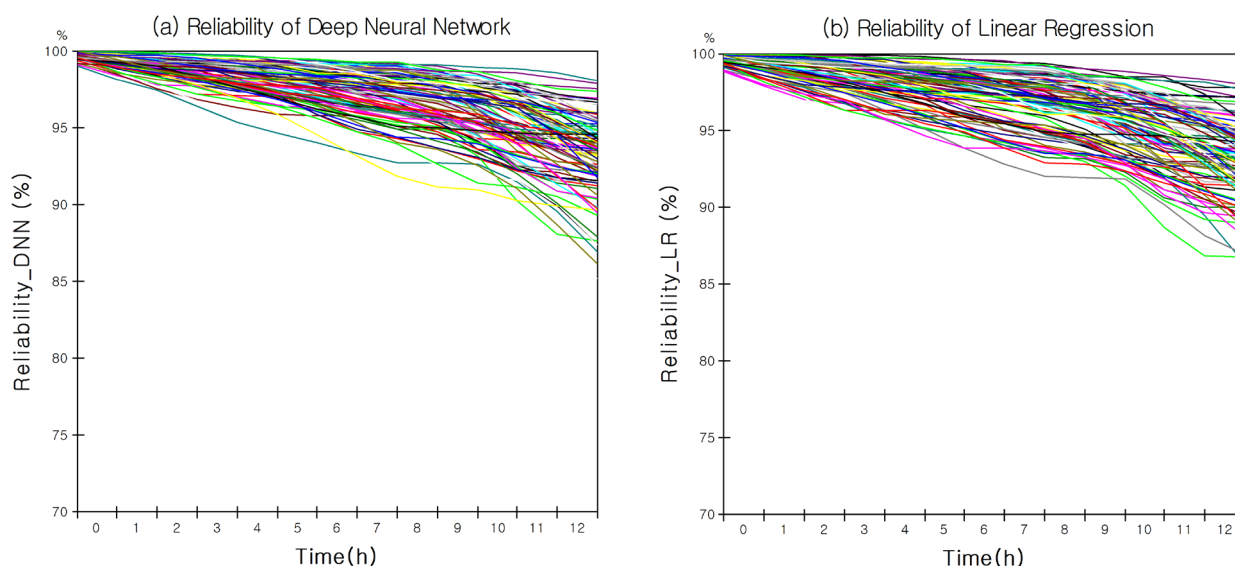
340   **Figure 5:** Training reliability by combining system dynamics and machine learning when predicting road temperature. (a) The graph means the reliability of the deep neural network by data acquisition date, and the average value is 93.01%. (b) The graph means the reliability of linear regression by data acquisition date, and the average value is 91.4%. The parameters of the DNN model and the LR model were optimised with the evolution algorithm.

After the training reliability was confirmed, it was derived by entering the test data into the DNN model. The DNN model
345 performance test was conducted for ground temperature from December 16–19, 2021, the scenario date described above, from
0:00 AM to 13:00 PM. Based on the error indicators, the model test results are listed in Table 5. Error and reliability values
were derived according to the error indicator, model type, and scenario date. In the case of LR results, if the previous study
method (Hong et al., 2021) could be introduced as it is, 98 datasets could be used. In the current study, 1498 datasets were
used; therefore, there was a difference in the results. Hence, DNN (1498 datasets), LR (1498 datasets), and LR (previous
350 studies, 98 datasets) were compared to analyse the superiority of the DNN model compared to linear regression. As a result,
the average RMSE of the DNN model was improved by 13.8% compared with the LR. In addition, the reliability (100-MAPE
× 100%) of the DNN model was 1.77% higher than that of the LR model. Compared to the previous study (LR, data set: 97),
the RMSE was improved by 148.6%, and the reliability was increased by 11.43%. Therefore, the DNN model had a higher
prediction performance than the LR model; thus, the prediction value of the DNN model for road temperature was used.

355

Table 5: System dynamics and machine learning results for road temperature prediction. The results were expressed as RMSE, MAPE, and
reliability of the model and actual data.

Error Indicator	Model Class (Train set)	12/16	12/17	12/18	12/19	Average
RMSE	DNN (1498)	1.07	0.72	1.14	1.42	1.09
	LR (1498)	1.25	0.75	1.42	1.55	1.24
	LR (98)	3.32	1.82	4.1	1.59	2.71
MAPE	DNN (1498)	0.05	0.04	0.06	0.08	0.06
	LR (1498)	0.07	0.05	0.07	0.1	0.07
	LR (98)	0.15	0.09	0.34	0.11	0.17
Reliability (1-MAPE) *100%	DNN (1498)	94.9%	96.45%	94.24%	92.39%	94.5%
	LR (1498)	92.87%	95.46%	92.1%	90.47%	92.73%
	LR (98)	85.15%	91.06%	66.29%	89.77%	83.07%

The average road temperature for December 16–19 predicted by the DNN model is shown in Figure 6. The lowest temperature
360 on 16 December was predicted to be –0.31 °C, and the maximum temperature was 10.46 °C. The minimum temperature on 17
December was predicted to be 0.48 °C, and the maximum temperature was 4.74 °C. The lowest temperature on 18 December
was predicted to be 0.17 °C, and the maximum temperature was 2.89 °C. The lowest temperature on 19 December was
predicted to be –0.73 °C, and the maximum temperature was 3.36 °C. The predicted values of road temperature and road
moisture were substituted into the model calculation process to predict the amount and location of the black ice.
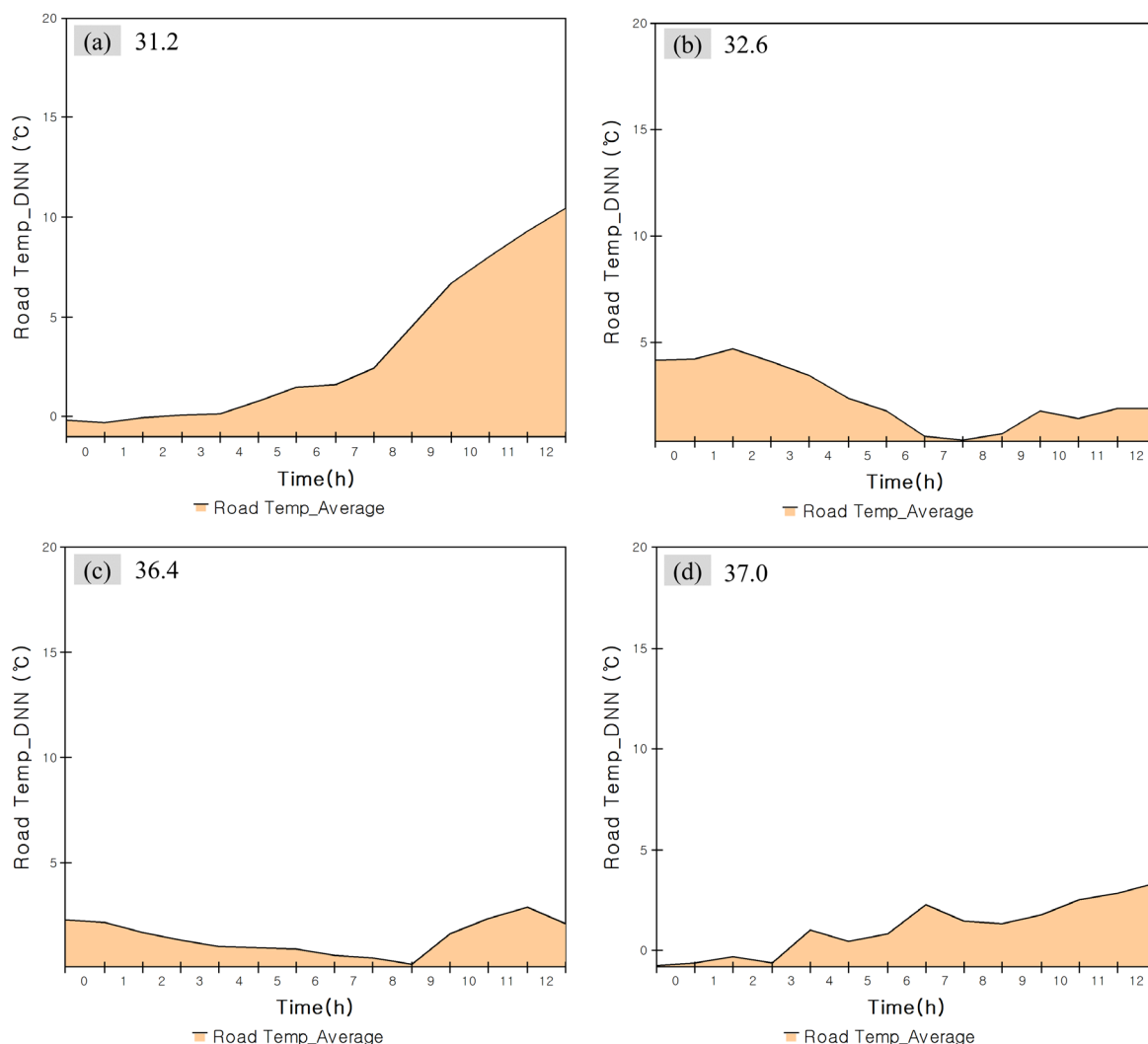
Figure 6: Road temperature prediction results by system dynamics and DNN. (a) Prediction of road temperature for December 16. (b) Prediction of road temperature for December 17. (c) Prediction of road temperature for December 18. (d) Prediction of road temperature for December 19.

Road moisture was modelled based on the dynamic characteristics of the system dynamics, and black ice generation was modelled based on the predicted road temperature. The details of this process are shown in Figure 7. All graphs in Figure 7 show the average of 15764 points on the Suncheon-Wanju Highway. Figure 7 (a)–(d) shows the amounts of precipitation, condensation, and road moisture. The maximum amount of road moisture on December 16, 17, 18, and 19 was predicted to be 2107.59, 0.12, 1502.61, and 487.21 g/m^2, respectively. On December 19, road moisture increased sharply as the accumulated snow melted. Figure 7 (e)–(f) shows the amount of black ice generated per hour due to "freezing" and "thawing". The maximum amount of black ice on December 16 was predicted to be 0.72 g/m^2; the black ice was formed before water accumulation due to precipitation. The maximum amount of black ice on December 17 was predicted to be 127.03 g/m^2, as a

result of freezing rain. The maximum amount of black ice on December 18 and 19 was predicted to be 14.36 and 17.91 g/m^2, respectively, which was a result of road moisture formed by the melting of accumulated snow. The model results of specific points (points corresponding to 31.2, 32.6, 36.4, and 37.0 of the highway milestones) among 15764 were compared with the
380   sensor data.

3.3 Black ice GIS simulation results

Figure 8 shows the simulation results of the amount and location of black ice predicted by the system dynamics modelling in GIS (Esri). The results of simulating the amount and location of black ice in units of 1 m^2 were exaggerated using the buffer function in GIS. Figure 8 (a)–(d) shows the predicted location and generated amount of black ice between December 16–19.
385   The raster information of each black ice map was the sum of the black ice generated from 00:00 AM to 13:00 PM on the selected day. The maximum amount black ice formed during the 14-h period was (a) 441 g/m^3, (b) 52,021 g/m^3, (c) 26,067 g/m^3, and (d) 9,770 g/m^3, respectively, for each scenario date and the total amount of black ice generated, i.e. the sum of all scenarios, was 88,300 g/m^3 [Figure 8 (e)]. The days with the highest amount of black ice were December 16 and 17, when freezing rain and snow occurred, respectively (Figure 8 (b) and (c), respectively), and it was found that road moisture was
390   higher and road temperature was lower than on the other days.

4 Discussion (Black ice model sensor validation)

To discuss the modelling and simulation results, sensor data were acquired, and comparative validation was performed. Three points in the top 2 levels and one point in the bottom 2 levels were selected from the black ice map in Figure 8 (e), which comprehensively covers all scenarios. Subsequently, the data were acquired from the sensor buried at the selected point. Multi-
395   sensor data were collected from December 16–19 and statistically compared and analysed with the model to verify the system dynamics model.

4.1 Black ice multi-sensor configuration

To determine the generation of black ice at the prediction point of the model, a black ice multi-sensor—that connects several sensors with the control board—was configured, as shown in Figure 9. The Multi-sensor consisted of a round force (FSR402),
400   water pressure (gravity: analog water pressure sensor), ultrasonic (W238), and temperature/humidity (SHT30). The round force sensor was buried in the floor, and it detected the pressure of the black ice generated from the upper part. The water pressure sensor had a principle similar to that of the round force sensor, and it detected the pressure of moisture that entered the upper part and was frozen inside. In the case of the ultrasonic sensor, the area where the ultrasonic wave was emitted faced the floor; when black ice was generated, a height difference (default of 8 cm) was detected. Finally, the temperature/humidity
405   sensor had a sensing part facing the ground, and the interval was ~ 2 cm.
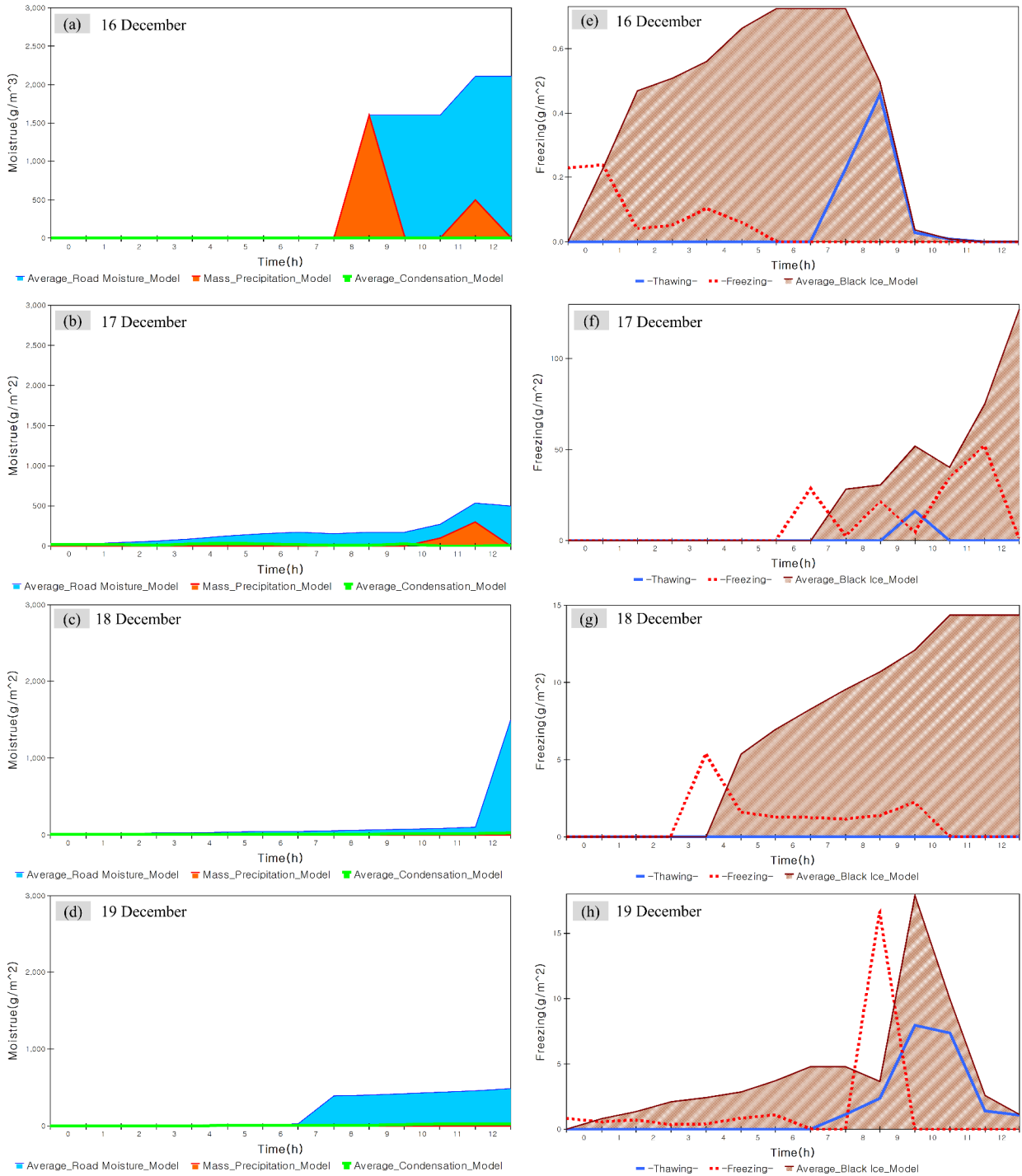
Figure 7: Prediction of road moisture and black ice through system dynamics model. (a), (b), (c), and (d) are the road moisture (calculated by condensation and precipitation) per Hour on the road from December 16–19. (d), (e), (f), and (g) are black ice (calculated by freezing, thawing) per Hour on the road from December 16–19.
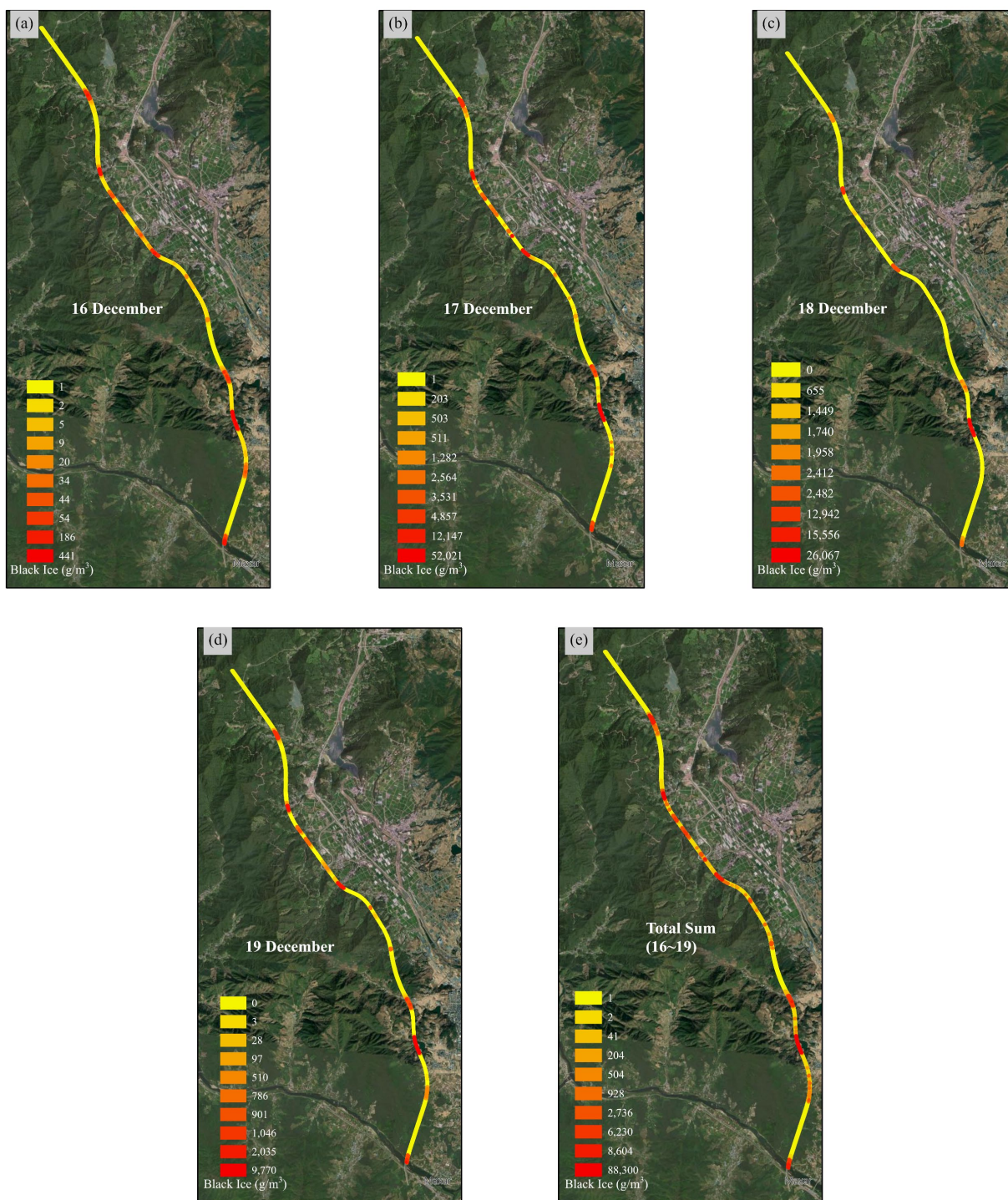
410

Figure 8: Simulation of black ice occurrence prediction results of system dynamics in units of 1 m² on GIS. (a), (b), (c), and (d) show the amount and location of black ice from December 16–19. (e) The sum of the amount and location of black ice from December 16–19. (Source: Esri, Maxar, Earthstar Geographics, and the GIS User Community.)
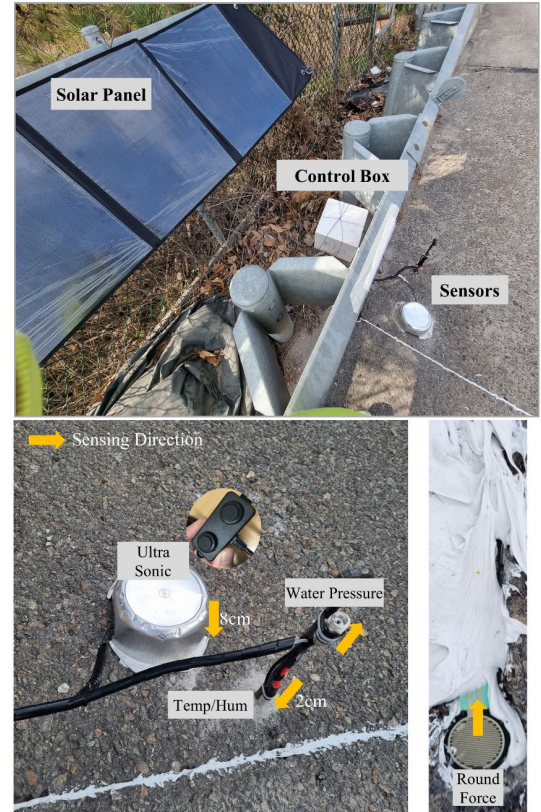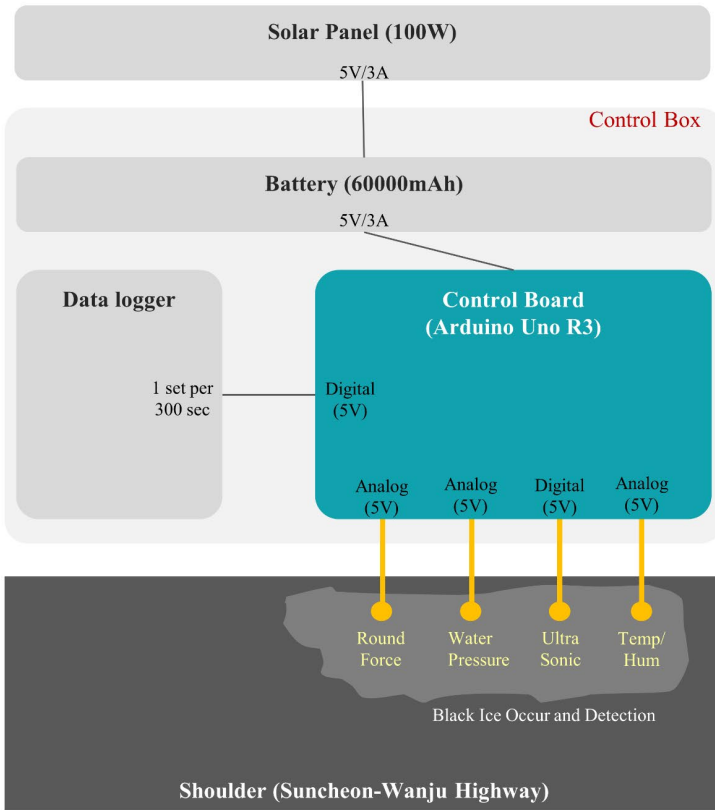
Figure 9: Configuration and installation photo of multi-sensor for black ice detection. Configuration and installation photo of multi-sensor for black ice detection. The sensing part of the round force and water pressure sensor faces upward, and the sensing part of the ultrasonic and temperature/humidity sensor faces downward.

4.2 Black ice data acquisition and model validation

After the black ice multi-sensor was positioned, data were acquired according to the scenario's date range (December 16–19). Points with signpost numbers 31.2, 32.6, 36.4, and 37.0 on the Suncheon-Wanju Highway were selected as burial points. Points 31.2, 32.6, and 37.0 corresponded to the top 2 levels of the amount of black ice prediction in Figure 8 (e), and points 36.4 corresponded to the bottom 2 levels. The data acquired by date at the corresponding points included the round force, water pressure, ultrasonic force, temperature, and humidity. A graph of the multi-sensor burial point and the received data is shown in Figure 10. For points 31.2, 32.6, and 37.0, data were acquired from December 16–19. For the 36.4 points set as the comparison group by the result of model prediction, data of December 16 were acquired owing to the field situation. The round force sensor was analysed through an upper-tailed test with model prediction results (Raftery et al., 1995). The water pressure sensor analysed the point where the frequency was constant using a fast Fourier transform to distinguish between the presence and absence of black ice (Rao et al., 2010). At point 36.4, where black ice was predicted to not occur, a signal with a constant frequency that is difficult to appear on ice was separated. The ultrasonic sensor was analysed through an upper-tailed test, such

430   as a round force sensor. It was assumed that the data for 36.4, the point where black ice was predicted to not occur, would be significantly different when other sensor data were used as the population. The temperature/humidity sensor was compared and analysed to determine whether it was consistent with other sensors when the temperature dropped or humidity increased.

The white noise of the multi-sensor waveforms in Figure 10 was corrected using a low-pass filter. In particular, the correction of white noise, which occurs mainly in analogue sensors, is essential for analysing data. The low-pass filter attenuates signals
435   above the cutoff frequency and passes only signals below a specific frequency. The mathematical contents are as follows in Eq. (19); where "τ" is a time constant, and the larger the value, the greater the data correction, but a time delay occurs. The final correction value (y_n) is calculated from the value corrected immediately before (y_{n-1}) and the target value to be corrected (x_n) (Kumngern et al., 2022; Roberts and Mullis, 1987).

$$y_n = \frac{\tau}{\tau + t_s} y_{n-1} + \frac{t_s}{\tau + t_s} x_n \qquad (19)$$

4.2.1 Round force sensor analysis

The round force sensor is the primary data that can determine the occurrence of black ice by time among the five sensors, and it was compared with the model by time unit. Figure 11 shows the buried position of the sensor and a graph comparing the sensor value and model. The graph in Figure 11 shows a visualisation of the model (system dynamics) and RF (round force) sensor superimposed results. It can be seen that the black ice occurrence range predicted by the model by point and time
445   roughly coincided with the period when the sensor detected black ice. For the convenience of observation, sensor data arranged with a low-pass filter were included in the graph, but the analysis was performed including white noise before attenuation. The time period is approximately the same, but the difference in the trend in the graph's height is because of the model representing the amount of black ice (g/m^3) and the sensor value being a force value (dimensionless). When the units and dimensions of the variables are different, a difference occurs in their maximum values. The data acquired at points 36.4 and 37.0 contain a certain
450   noise pattern. It is interpreted that this is not an occurrence of black ice but an electrical error caused by the attachment of multiple sensors. An analysis was performed considering this phenomenon.

The Z-test (upper tailed test) was performed to analyse the graph in more detail on the RP sensor values detected in the time range that predicted black ice in the model. The P-value derived from the Z-test result is the probability value that the research model indicates null hypothesis to be correct but is wrong and is the probability that a specific alternative hypothesis will result
455   in a type I error (error indicating that the null hypothesis is correct but is wrong). If the research hypothesis is tested with a 95% confidence level, the significance level is set to 0.05 (α, 5%). If the p-value is less than 0.05, the null hypothesis is rejected, and the alternative hypothesis is adopted. The null and alternative hypotheses were established, and the p-value was calculated to confirm whether the alternative hypothesis (research hypothesis) was acceptable (Raftery et al., 1995).

H0 (null hypothesis): The value of the round force sensor in the range predicted by the model is not different from other periods.
460   H1 (alternative hypothesis): The value of the round force sensor in the range predicted by the model is higher than that in other periods.
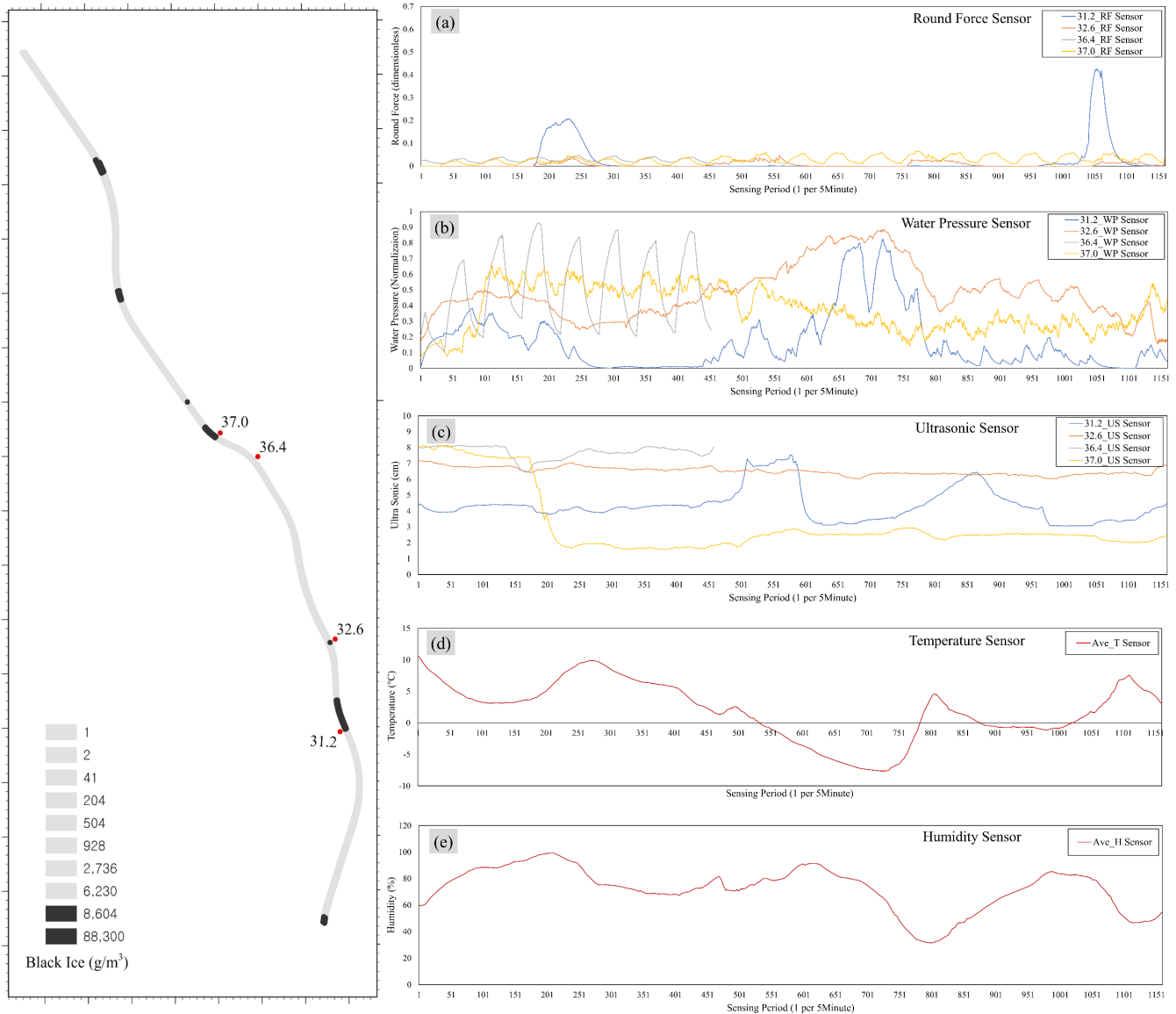
Figure 10: The location of occurrence of black ice (top 2 levels) and data collection results for each sensor. Points 31.2, 32.6, and 37.0 are the experimental group, and points 36.4 are the comparison group. (a) Data graph of the round force sensor. (b) Data graph of the water pressure sensor. (c) Data graph of ultrasonic sensor. (d) Average of temperature from temperature/humidity sensor. (e) Average of humidity from temperature/humidity sensor.

The formula used to obtain the standardised Z-score of the performance value X of the sample data is as follows in Eq. (18), where X is the round force sensor value variable, μ is the population mean for the sensor value, σ is the population standard deviation, and n is the number of variables. The results of the upper-tailed test are shown in Table 6. The three points (31.2, 32.6, and 37.0) where black ice was predicted to occur had a P-value lower than 0.05, so the null hypothesis was rejected, and the alternative hypothesis was adopted. It was interpreted that black ice occurred significantly at the corresponding point.
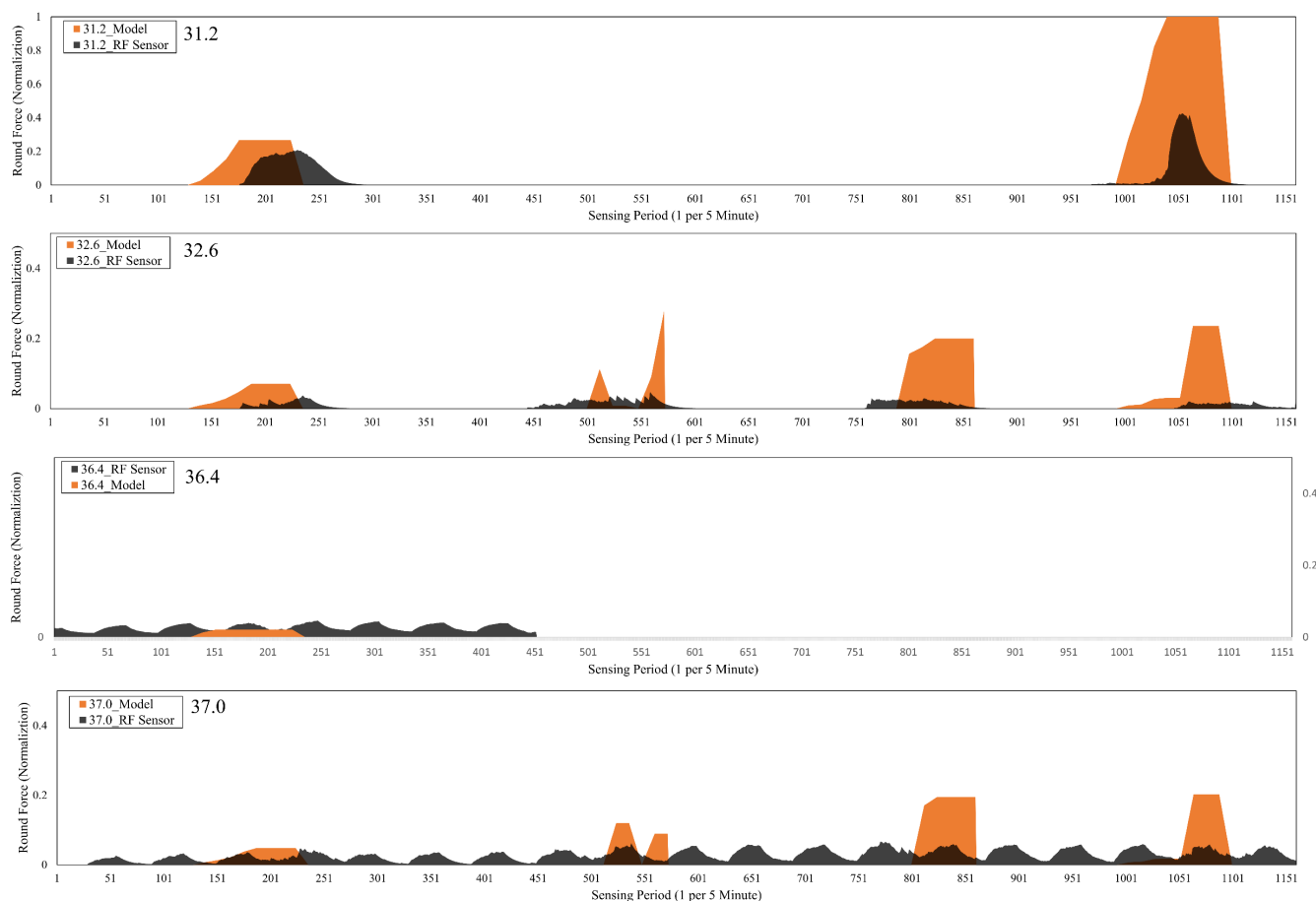
Figure 11: Comparison graph of the data value of round force sensor and black ice prediction value of system dynamics model.

At point 37.0, where black ice was predicted to not occur, the P-value was higher than 0.05; therefore, it was interpreted that
475 black ice would not occur. Accordingly, it was confirmed that the round force sensor value and model result were the same, and the validity was verified.

$$Z = \frac{X - \mu}{\frac{\sigma}{\sqrt{n}}} \tag{20}$$

Table 6: Z-test (upper-tailed test) result of round force sensor data value.

Section	Black Ice occur	Population Mean	Z-score	P-Value (One-Tailed)	Test Results
31.2	occur	0.00268	111.676	about 0 (<α)	H1 adoption
32.6	occur	0.00266	22.40736	about 0 (<α)	H1 adoption
36.4	non-occur	0.02645	0.55702	0.28868(>α)	H0 adoption

37.0	occur	0.02698	2.79609	0.00258(<α)	H1 adoption

4.2.2 Water pressure sensor analysis

480 Figure 10 (b) shows a graph of water pressure, and voltage—which is a raw data value—was normalised to a value from 0 to 1 for ease of analysis. The graph of water pressure used a fast Fourier transform (FFT) to analyse the frequency trend and then determined whether black ice occurred by searching for a fixed frequency. FFT is an algorithm that rapidly calculates the discrete Fourier transform (DFT). DFT is as in Eq. (21). By decomposing a series of values into different frequencies, it is possible to check the waveforms of several trigonometric functions mixed in one signal. Although this operation is useful in

485 many engineering fields, the direct calculation is not efficient; therefore, it is performed using FFT. The FFT quickly computes a transformation by factoring the DFT matrix into a product of sparse factors (Rao et al., 2010).

$$H_n = \frac{1}{N} \sum_{m=0}^{n-1} h_n e^{\left(-\frac{2\pi i}{N}mn\right)}, (0 \leq n \leq N - 1) \qquad (21)$$

Figure 12 shows the result of the fast Fourier transformation of the graph of the water pressure based on time. Figure 12 (a), (b), and (d) show FFT graphs of points predicting that black ice will occur in the model, and Figure 12 (c) shows FFT graphs

490 of points predicting that black ice will not occur in the model. The x-axis represents the frequency of the FFT graph (S, Hz) and the y-axis represents the amplitude. The FFT separates the periodic wavelengths in the signal in the frequency domain. It is assumed that if ice, not water, is frozen in the water pressure sensor, periodic wavelengths of relatively high frequencies can be observed. Therefore, at 0.00001 Hz (sample time: 300 sec) in the graph of Figure 12 (c), a sharp increase in amplitude was observed (0.27). A consistent waveform was observed at the indicated point in Figure 12 (c), the control group, unlike the

495 other points according to the amplitude value. It can be assumed that this is a property of the liquid that is not subjected to time-dependent stress owing to ice. At points 31.2, 32.6, and 37.0, where inconsistent wavelength was observed, irregular stress was generated due to ice, which was presumed to be compatible with the model results. At point 37.0, where a consistent wavelength was observed, no irregular stress was observed; therefore, it was presumed to be compatible with the model results.

4.2.3 Ultrasonic sensor analysis

500 Figure 10 (c) shows an ultrasonic graph. The ultrasonic sensor data started with an initial value of 8 cm and decreased when the ice changed the height of the ground surface. It was hypothesised that the sensor value of 36.4, the point where black ice was predicted to not occur, would be significantly larger than the 31.2, 32.6, and 37.0 points predicted as the occurrence of black ice. The established hypothesis was tested using the Z-test (upper-tailed test) for the alternative hypothesis (research hypothesis). The null and alternative hypotheses for point 36.4, the comparison group, are as follows:
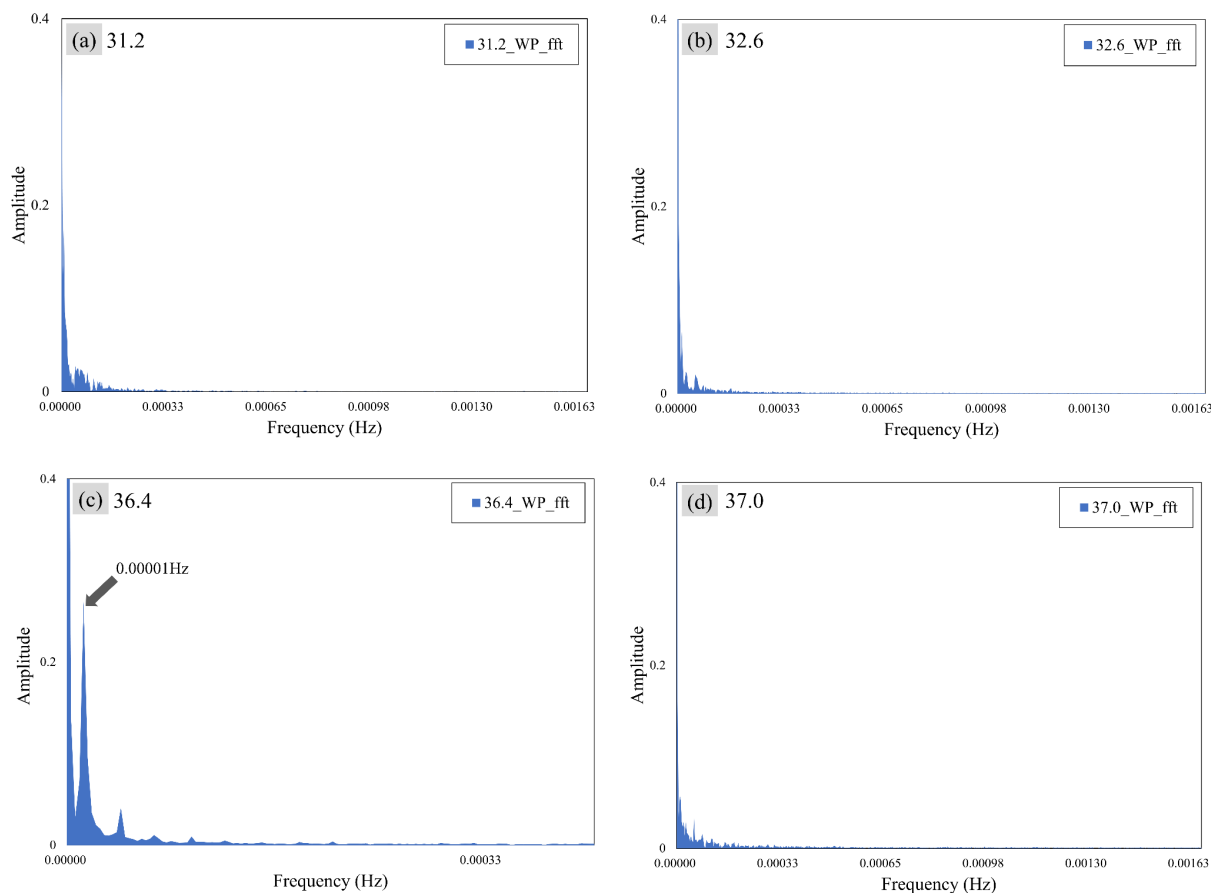
Figure 12: Fast Fourier transform the result of the data signal of the water pressure sensor. (a), (b), and (d) indicate points where the system dynamics model predicted that black ice would occur, and no waveforms of a particular period were observed. (c) indicates the point where the system dynamics model predicted that black ice did not occur, and a waveform of a particular period was observed.

H0 (null hypothesis): The ultrasonic value of the point predicted by the model as non-occurrence is not different from the point predicted by the occurrence.

H1 (alternative hypothesis): The ultrasonic value of the point predicted by the model as non-occurrence is different from that predicted as the occurrence.

As in the round force sensor analysis, if the p-value is less than the significance level of 0.05, the null hypothesis is rejected, and the alternative hypothesis is adopted. The result of the upper tailed test of the sample data at point 36.4 indicated a population mean of 4.67, standard deviation of 1.91, Z-score of 34.17928, and P-value of less than 0.00001. Since the P-value was lower than the significance level ($\alpha = 0.05$), H0 (null hypothesis) was rejected, and H1 (alternative hypothesis) was adopted. According to the adoption of the alternative hypothesis, a research hypothesis is established: the ultrasonic value of the point predicted by the model as non-occurrence is different from the point predicted as the occurrence. Their contents are summarised in Table 7. Since the points 31.2, 32.6, 36.4 are the population and the point 36.4 is the sample, the hypothesis test was performed only on point 36.4 (Raftery et al., 1995).

Table 7: Z-test (upper-tailed test) result of ultrasonic sensor data value.

Section	Black Ice occur	Sensor Mean (cm)	Z-score	P-Value (One-Tailed)	Test Results
31.2	occur	4.36	-	-	-
32.6	occur	6.51	-	-	-
36.4	non-occur	7.71	34.17928	About 0 ($<\alpha$)	H1 adoption
37.0	occur	3.09	-	-	-

4.2.4 Temperature/humidity sensor and multi-sensor analysis

Figure 13 shows the average graph for the 31.2, 32.6, and 37.0 points where black ice significantly occurred among the round force, temperature, and humidity data. The highlighted bright areas (a)–(d) are time sections where black ice occurred in the system dynamics model. Figure 13 shows three graphs. (A) is a round force sensor, (B) is a temperature/humidity sensor, and (C) is precipitation (mm) and snow cover (cm) data obtained from the ASOS of the Korea Meteorological Administration for additional comparative analysis: (a), the average humidity exceeded 100%, and the average temperature was a minimum of 2.98 °C. As previously analysed, this is an environment in which dew is formed by fog, and because all the points where black ice occurred significantly are near bridges, freezing occurred even at the temperature mentioned in the image. In the case of time; (b), it was found that black ice occurred because the temperature dropped to –3.28°C at the lowest, with freezing rainfall; (c), as shown in graph (C), snow cover was observed. As in (B), black ice occurred due to the low temperature of the road surface after the snow melted in the section where the temperature rose to a maximum of 6.25 °C. The snow cover exists in (d) as in (c); and (d), the snow that melted when the temperature rose to a maximum of 9.04 °C was frozen again at a low temperature. In conclusion, an environment prone to ice formation was observed when the model predicted that black ice would occur. In addition, in the round force graph in Figure 13, the 31.2, 32.6, and 37.0 points were consistent with the model and the black ice occurrence trend. Temperature and humidity also created an environment that simultaneously formed black ice.

Table 8 shows the analysis results of the multi-sensor, a concept that includes both temperature/humidity and the sensors (round force, water pressure, ultrasonic) described above. Table 8 briefly shows the analysis results for the 31.2, 32.6, 36.4, and 37.0 points and sensors. At the 31.2, 32.6, and 37.0 points where back ice occurrence was predicted by the model, the Z-test result of round force was "High", the fast Fourier transform result of water pressure was "Aperiodic", the Z-test result of ultrasonic was "Low", and temperature/humidity was "Associated", implying "Occur" of black ice. At the 36.4 point where it was predicted that black ice does not occur, the Z-test result of round force was "Low," fast Fourier transform result of water pressure was "Periodic", ultrasonic Z-test result was "High", temperature/humidity was "Un-associated", implying "Non-occur" of black ice.
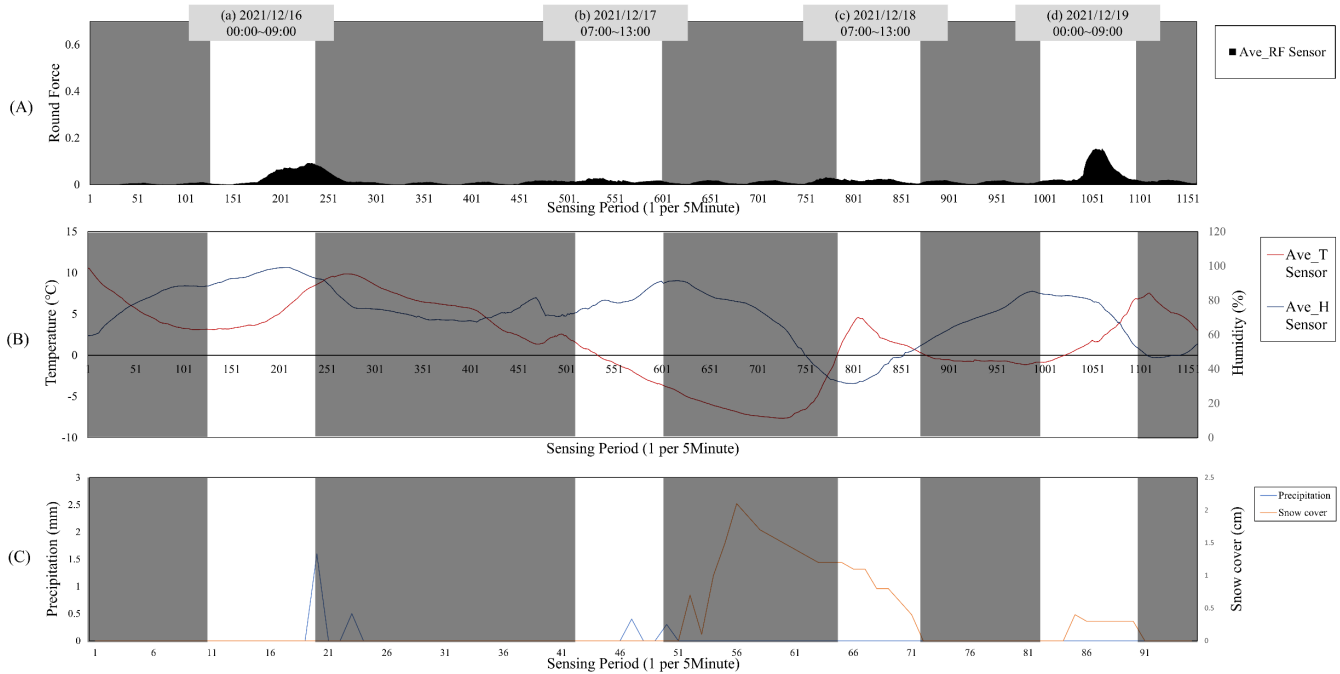
Figure 13: Data analysis result of temperature/humidity sensor. Round force, temperature/humidity, precipitation, and snow cover were compared.

Table 8: Comprehensive analysis result of multi-sensor.

Section	Round Force		Water Pressure		Ultrasonic		Temperature/ Humidity	Match the model
	Result (Z-Test)	Black Ice	Result (FFT)	Black Ice	Result (Z-Test)	Black Ice	Significance	
31.2	High	Occur	Aperiodic	Occur	Low	Occur	Associated	matched
32.6	High	Occur	Aperiodic	Occur	Low	Occur	Associated	matched
36.4	Low	Non-occur	Periodic	Non-occur	High	Non-occur	Un-associated	matched
37.0	High	Occur	Aperiodic	Occur	Low	Occur	Associated	matched

5 Conclusion

This study modelled the amount and location of black ice using the system dynamics method and simulated it using GIS. The amount of black ice generated per unit area (1 m²) was obtained as a block diagram constructed using the causal relationship between factors in the system dynamics model. The information input to the system dynamics model was

meteorological and spatial data, and road temperature and moisture were calculated using these data. The road temperature
was modelled using a DNN model and an evolution algorithm, and the road moisture was modelled numerically. Finally, the
amount and location of black ice were predicted through numerical modelling combining road temperature and road moisture
and simulated in 1 m^2 units on GIS. The study area was the Suncheon-Wanju highway in Gurye-gun, Jeollanam-do, and
modelling and simulations were performed from December 16–19.

Based on the simulation results, multiple sensors were positioned at 31.2, 32.6, 36.4, and 37.0 points on the Suncheon-
Wanju highway, and data were collected. Multi-sensor consisted of a round force, water pressure, ultrasonic force, temperature,
and humidity, and each sensor was analysed through a Z-test and fast Fourier transform. For round force, using the Z-test
(upper-tailed test) through the P-Value, it was tested whether the predicted point where black ice would occur on the model
matched the sensor value. Water pressure was used to analyse the surging value of the amplitude in the frequency domain
using a fast Fourier transform to determine whether ice existed according to the periodic vibration. Ultrasonic Z-tests were
performed using the P-value. It was verified that the height value of the comparison group (36.4 points) was significantly
higher than that of the other points (31.2, 32.6, 37.0 points). Finally, the temperature and humidity were analysed at the point
where black ice was predicted to occur in the model. In addition, the causal relationship between the round force analysed
previously, and precipitation and snow cover data obtained from the AWS of the Korea Meteorological Agency was
comparatively analysed.

This study predicted the amount and location of black ice using system dynamics and GIS. However, the prediction value
of occurrence does not reflect other characteristics of traffic accidents related to society and the environment; therefore, it is
not a complete concept to approach vulnerability. Hence, additional research on traffic accident vulnerability and risk is
required. In addition, in the case of sensor technology, because the round force sensor is directly buried in the road shoulder,
the actual occurrence trend of black ice can be checked over time; however, water pressure and ultrasonic sensors have different
data collection environments (water pressure: collected inside the metal sensor, ultrasonic: cap to prevent snow accumulation).
Therefore, it is possible to compare the experimental group (31.2, 32.6, and 37.0) and the comparison group (36.4) in the
overall time, but the comparison at each time point is a matter to be further developed. Despite few shortcomings, the results
of this study can provide useful data for government agencies (e.g. road traffic authorities) when managing traffic accidents
caused by black ice. It should be noted that major factors have been added to the existing studies, the road temperature
prediction rate has been improved by combining the DNN technique with system dynamics, and the system dynamics model
has been verified using a multi-sensor. In the future, if various factors are supplemented for society and the environment and
a more accurate vulnerability and risk assessment is performed, it is possible to reduce the manpower wasted in the
investigation by selecting the points where damage is expected from black ice in advance. It is also possible to apply structural
or non-structural countermeasures at more precise points.

Appendix A: Block diagram structure and model definition of the system dynamics model

585
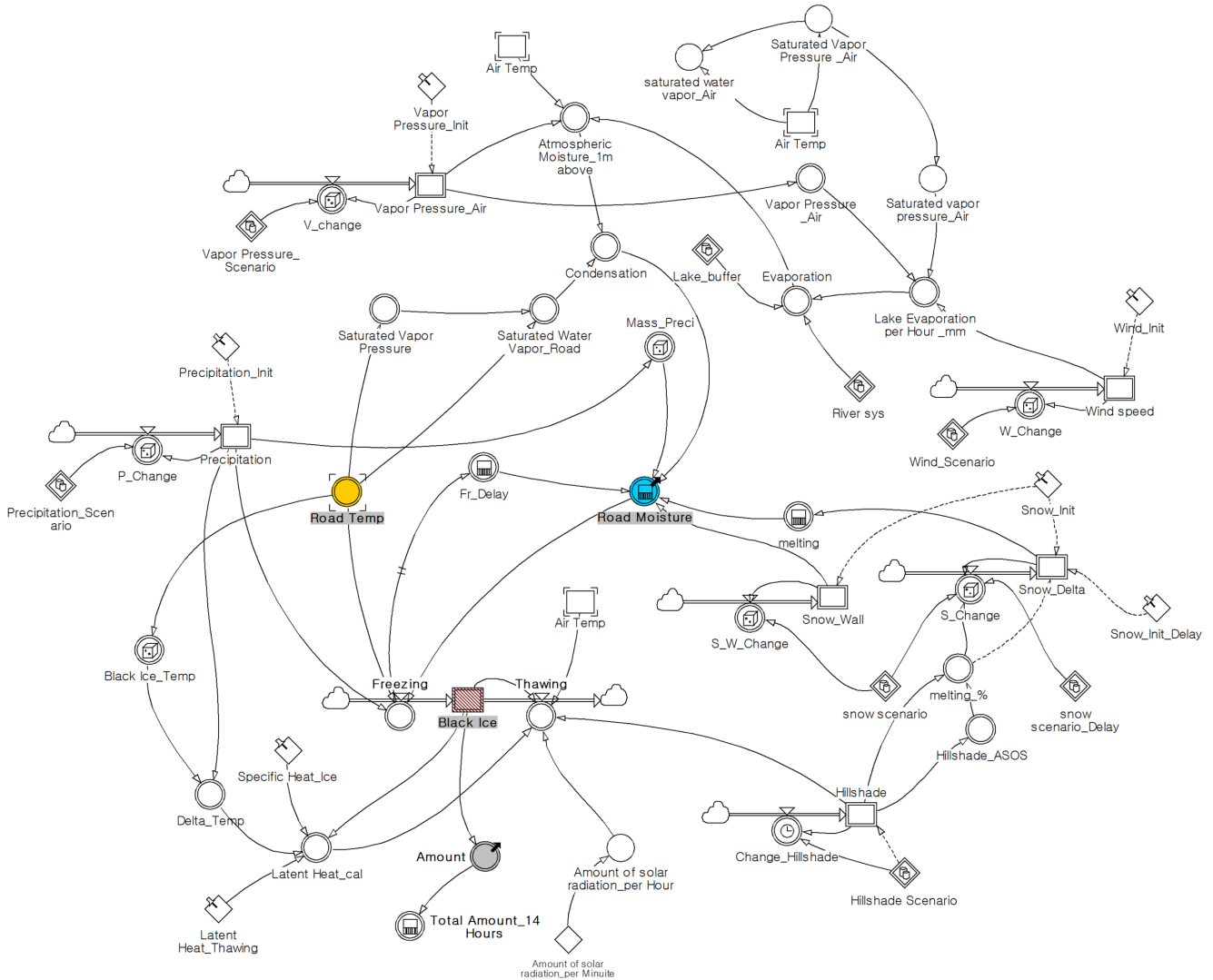
Figure A1: Block diagram of the system dynamics model.

Table A1: The primary definition of a model.

Number	Name	Definition
1	RMSE DNN	SQRT(RUNSUM(('Road Temp_Trure'-'Road Temp_Predict_DNN')^2)/14)
2	RMSE LR	SQRT(RUNSUM(('Road Temp_Trure'-'Road Temp_Predict_LR')^2)/14)
3	Condensation	MAX(0, Atmospheric Moisture_1m above- Saturated Water Vapor _Road)

4	Road Moisture	MAX(0,RUNSUM(Condensation+Mass_Preci-Fr_Delay))+IF(Snow_Wall=0,melting,0)
5	Lake Evaporation per Hour (mm)	MAX(0,(0.345*(' Saturated Vapor Pressure_Air_mmhg'-' Vapor Pressure _Air_mmhg')*(0.5+0.54*'Wind Speed'))/24)
6	Freezing	IF('Road Moisture'<0,0,1)*IF(Precipitation>0,'Road Moisture'*IF('Road Temp'<=1,1,0),'Road Moisture'*IF('Road Temp'<=0,1,0))
7	Thawing	IF('Air Temp'>0,MIN(1,(((Hillshade/250)*' Amount of solar radiation_per Hour') DIVZ0 'Latent Heat_cal'))*'Black Ice',0)
8	MAPE	FOR(i=1..15765|RUNSUM(ABS(('Road Temp_Predict_nor - Copy'[i]-'Road Temp_Trure_nor - Copy'[i])/('Road Temp_Predict_nor - Copy'[i]))/14))*100%
9	Mass of Precipitation	FOR(i=1..15765|RANDOM (0.98, 1.02, 0.5/i)) * (100*100*Precipitation*0.1)
10	Road Temperature	'lf4-1'+Weight_Bridge*Loacation_Bridge+6.5*((1+Snow_Wall)/(1+Snow_wall_max))-IF(Hillshade>0,3.5*(Hillshade/250),0)
11	Saturated Vapor Pressure (Road)	6.1078*10^(7.5*'Road Temp'/('Road Temp'+237.3))
12	Saturated Vapor Pressure (Air)	6.1078*10^(7.5*'Air Temp'/('Air Temp'+237.3))
13	Saturated Water Vapor (Air)	217*('Saturated Vapor Pressure _Air'/('Air Temp'+273.15))
14	Saturated Water Vapor (Road)	217*('Saturated Vapor Pressure _Road' /('Road Temp'+273.15))
15	Atmospheric Moisture (1m above)	217*('Vapor Pressure'/('Air Temp'+273.15))+ 'Evaporation g per m3'
16	Evaporation (g/m3)	100*100*' Lake Evaporation per Hour _mm'*0.1*'River Sys'
17	Weight_Bridge	-1-(1*(TIME/13)) //-(((TIME+3)/16)*2)// //IF(TIME<9,-1,IF(TIME<14,-2,0))
18	Latent Heat_cal	'Specific Heat_Ice'*'Black Ice'*ABS(Delta_Temp)+'Latent Heat_Thawing'*'Black Ice'*ABS(Delta_Temp)
19	Amount of solar radiation_per Hour	'Amount of solar radiation_per Minuite'*10000*60
20	S_Change	FOR(i=1..15765|RANDOM (0.98, 1.02, 0.5/i)) *IF(('snow scenario_Delay'[INDEX(INTEGER(NUMBER(TIME)+1))]-'snow scenario'[INDEX(INTEGER(NUMBER(TIME)+1))])>0,('snow scenario_Delay'[INDEX(INTEGER(NUMBER(TIME)+1))]-'snow scenario'[INDEX(INTEGER(NUMBER(TIME)+1))]),0)*'melting_%'-Snow_Delta
21	Melting	RUNSUM((100*100*Snow_Delta)*0.92*0.1)

Data availability

590   The data sources used for the case studies are listed in Table 4.

Author contributions

SBH, JK were involved in the conceptualization; HSY, SKY developed the methodology; HSY supervised SBH and JK in the spatial and meteorological data processing; SBH explored the system dynamics modelling system and prepared input data; JK performed the connectivity analysis; SKY and SYR analysed the data; SBH and SYR developed the algorithm for data analysis
595 and visualization; ISJ wrote the manuscript draft and edited the coauthors revisions; all co-authors were involved in the review of the manuscript.

Competing interests

The authors declare that they have no conflict of interest.

Acknowledgements

600 This paper was supported by "Ministry of the Interior and Safety" R&D program(20017423)

References

Ali, S., Biermanns, P., Haider, R., and Reicherter, K.: Landslide susceptibility mapping by using a geographic information system (GIS) along the China–Pakistan Economic Corridor (Karakoram Highway), Pakistan, Natural Hazards and Earth System Sciences, 19, 999-1022, 10.5194/nhess-19-999-2019, 2019.

605 An, J. S. and Choi, S. W.: The role of winter weather in the population dynamics of spring moths in the southwest Korean peninsula, J. Asia-Pac. Entomol., 16, 49-53, 10.1016/j.aspen.2012.08.005, 2013.

Traffic Accident Analysis System: http://taas.koroad.or.kr/web/shp/adi/initBasisPurps.do?menuId=WEB_KMP_IID_IID_PAB, last access: January 1, 2020.

Bardou, E. and Delaloye, R.: Effects of ground freezing and snow avalanche deposits on debris flows in alpine environments,
610 Natural Hazards and Earth System Sciences, 4, 519-530, 2004.

Bezrukova, N., Stulov, E., and Khalili, M.: A model for road icing forecast and control, Proc. SIRWEC (conference), Turin, ITALY, 25th-27th March, 2006, 50-57,

Bonanno, R., Loglisci, N., Cavalletto, S., and Cassardo, C.: Analysis of Different Freezing/Thawing Parameterizations using the UTOPIA Model, Water, 2, 468-483, 2010.

615 Cary, L.: Black ice, Vintage, New York, USA2010.

Chapman, L., Thornes, J. E., and Bradley, A. V.: Modelling of road surface temperature from a geographical parameter database. Part 2: Numerical, Meteorological Applications, 8, 421-436, 2001.

Cheng, C., Auld, H., Li, G., Klaassen, J., and Li, Q.: Possible impacts of climate change on freezing rain in south-central Canada using downscaled future climate scenarios, Natural Hazards and Earth System Sciences, 7, 71-87, 2007.

620 De Myttenaere, A., Golden, B., Le Grand, B., and Rossi, F.: Mean absolute percentage error for regression models, Neurocomputing, 192, 38-48, 2016.

World_Imagery: https://services.arcgisonline.com/ArcGIS/rest/services/World_Imagery/MapServer, last access: January 20.

World Hillshade: https://services.arcgisonline.com/arcgis/rest/services/Elevation/World_Hillshade/MapServer, last access: January 20.

625 Forrester, J. W.: System dynamics, systems thinking, and soft OR, System dynamics review, 10, 245-256, 1994.

Hayward, M. W., Whittaker, C. N., Lane, E. M., Power, W. L., Popinet, S., and White, J. D. L.: Multilayer modelling of waves generated by explosive subaqueous volcanism, Natural Hazards and Earth System Sciences, 22, 617-637, 10.5194/nhess-22-617-2022, 2022.

Holland, J. H.: Genetic algorithms and adaptation, in: Adaptive Control of Ill-Defined Systems, Springer, 317-333, 1984.

630 Hong, S.-B., Lee, B.-W., Kim, C.-H., and Yun, H.-S.: System Dynamics Modeling for Estimating the Locations of Road Icing Using GIS, Applied Sciences, 11, 8537, 2021.

Hull, C.: 'Black Ice and Frozen Rain', Poetry-Rev., 89, 23-24, 1999.

Jeong, D. I., Cannon, A. J., and Zhang, X.: Projected changes to extreme freezing precipitation and design ice loads over North America based on a large ensemble of Canadian regional climate model simulations, Natural Hazards and Earth System

635 Sciences, 19, 857-872, 10.5194/nhess-19-857-2019, 2019.

Traffic accident article (case4): http://www.joynews24.com/view/1231389, last access: December 26, 2019.

Kämäräinen, M., Hyvärinen, O., Jylhä, K., Vajda, A., Neiglick, S., Nuottokari, J., and Gregow, H.: A method to estimate freezing rain climatology from ERA-Interim reanalysis over Europe, Natural Hazards and Earth System Sciences, 17, 243-259, 10.5194/nhess-17-243-2017, 2017.

640 Kangas, M., Heikinheimo, M., and Hippi, M.: RoadSurf: a modelling system for predicting road weather and road surface conditions, Meteorological applications, 22, 544-553, 2015.

Kelleher, J. D.: Deep learning, MIT press2019.

Kim, C. H.: SYSTEM DYNAMICS, pybook, Seoul, Korea2021a.

Traffic accident article (case1): https://www.yna.co.kr/view/AKR20210210121400530, last access: April 27, 2022.

645 Traffic accident article (case5): https://www.segye.com/newsView/20191129511652?OutUrl=naver, last access: 29 November 2019.

KMA Weather Data Service - Open MET Data Portal: https://data.kma.go.kr/cmmn/main.do, last access: December 11, 2020.

Koumoutsaris, S.: A hazard model of sub-freezing temperatures in the United Kingdom using vine copulas, Natural Hazards and Earth System Sciences, 19, 489-506, 10.5194/nhess-19-489-2019, 2019.

650 Kumngern, M., Khateb, F., and Kulej, T.: 0.5 V Current-Mode Low-Pass Filter Based on Voltage Second Generation Current Conveyor for Bio-Sensor Applications, Ieee Access, 10, 12201-12207, 10.1109/access.2022.3146328, 2022.

Traffic accident article (case3): http://news.tvchosun.com/site/data/html_dir/2020/01/06/2020010690068.html, last access: January 6, 2020.

Lee, Y.-M., Oh, S.-Y., and Lee, S.-J.: A study on prediction of road freezing in Jeju, Journal of Environmental Science

655 International, 27, 531-541, 2018.

Liu, S. J., Nazarian, N., Hart, M. A., Niu, J. L., Xie, Y. X., and de Dear, R.: Dynamic thermal pleasure in outdoor environments - temporal alliesthesia, Sci. Total Environ., 771, 10, 10.1016/j.scitotenv.2020.144910, 2021.

Liu, T., Pan, Q., Sanchez, J., Sun, S., Wang, N., and Yu, H.: Prototype Decision Support System for Black Ice Detection and Road Closure Control, IEEE Intelligent Transportation Systems Magazine, 9, 91-102, 10.1109/mits.2017.2666587, 2017.

660 Mitra, R., Naruse, H., and Fujino, S.: Reconstruction of flow conditions from 2004 Indian Ocean tsunami deposits at the Phra Thong island using a deep neural network inverse model, Nat. Hazards Earth Syst. Sci., 21, 1667-1683, 10.5194/nhess-21-1667-2021, 2021.

Park, M.-S., Joo, S. J., and Son, Y. T.: Development of road surface temperature prediction model using the Unified Model output (UM-Road), Atmosphere, 24, 471-479, 2014.

665 Peng, Y. Z., Gong, D. Q., Deng, C. Y., Li, H. Y., Cai, H. G., and Zhang, H.: An automatic hyperparameter optimization DNN model for precipitation prediction, Appl. Intell., 52, 2703-2719, 10.1007/s10489-021-02507-y, 2022.

Pradhan, N. R., Downer, C. W., and Marchenko, S.: Catchment Hydrological Modeling with Soil Thermal Dynamics during Seasonal Freeze-Thaw Cycles, Water, 11, 116, 2019.

Raftery, A. E., Gilks, W., Richardson, S., and Spiegelhalter, D.: Hypothesis testing and model, Markov chain Monte Carlo in

670 practice, 1, 165-187, 1995.

Rao, K. R., Kim, D. N., and Hwang, J. J.: Fast Fourier transform: algorithms and applications, Springer2010.

Rathke, J. M. and McPherson, R. A.: 4A. 9 MODELING ROAD PAVEMENT TEMPERATURES WITH SKIN TEMPERATURE OBSERVATIONS FROM THE OKLAHOMA MESONET, 2006.

Roberts, R. A. and Mullis, C. T.: Digital signal processing, Addison-Wesley Longman Publishing Co., Inc.1987.

675   Sass, B. H.: A Numerical Model for Prediction of Road Temperature and Ice, Journal of Applied Meteorology, 31, 1499-1506, 10.1175/1520-0450(1992)031<1499:Anmfpo>2.0.Co;2, 1992.

Shao, J. and Lister, P.: The prediction of road surface state and simulation of the shading effect, Boundary-Layer Meteorology, 73, 411-419, 1995.

Silberberg, M. S. M. S.: Chemistry : the molecular nature of matter and change, McGraw-Hill, New York, USA2009.

680   Sterman, J.: Business Dynamics, McGrawHill, New York, USA2000.

Tabatabai, H. and Aljuboori, M.: A Novel Concrete-Based Sensor for Detection of Ice and Water on Roads and Bridges, Sensors, 17, 23, 10.3390/s17122912, 2017.

Teke, M. and Duran, F.: The design and implementation of road condition warning system for drivers, Measurement and Control, 52, 985-994, 2019.

685   Terzi, S., Sušnik, J., Schneiderbauer, S., Torresan, S., and Critto, A.: Stochastic system dynamics modelling for climate change water scarcity assessment of a reservoir in the Italian Alps, Natural Hazards and Earth System Sciences, 21, 3519-3537, 10.5194/nhess-21-3519-2021, 2021a.

Terzi, S., Sušnik, J., Schneiderbauer, S., Torresan, S., and Critto, A.: Stochastic system dynamics modelling for climate change water scarcity assessment of a reservoir in the Italian Alps, Nat. Hazards Earth Syst. Sci., 21, 3519-3537, 10.5194/nhess-21-

690   3519-2021, 2021b.

Toma-Danila, D., Armas, I., and Tiganescu, A.: Network-risk: an open GIS toolbox for estimating the implications of transportation network damage due to natural hazards, tested for Bucharest, Romania, Natural Hazards and Earth System Sciences, 20, 1421-1439, 10.5194/nhess-20-1421-2020, 2020.

Troiano, A., Pasero, E., and Mesin, L.: New system for detecting road ice formation, IEEE Transactions on Instrumentation

695   and Measurement, 60, 1091-1101, 2010.

Wang, S., Mu, L., Yao, Z., Gao, J., Zhao, E., and Wang, L.: Assessing and zoning of typhoon storm surge risk with a geographic information system (GIS) technique: a case study of the coastal area of Huizhou, Natural Hazards and Earth System Sciences, 21, 439-462, 10.5194/nhess-21-439-2021, 2021.

Jirisan From Wikipedia, the free encyclopedia: https://en.wikipedia.org/wiki/Jirisan, last access: April 27, 2022.

700   Xu, H., Zheng, J., Li, P., and Wang, Q.: Road icing forecasting and detecting system, AIP Conference Proceedings, 020089,

Xue, J. Q., Lin, J. H., Briseghella, B., Tabatabai, H., and Chen, B. C.: Solar Radiation Parameters for Assessing Temperature Distributions on Bridge Cross-Sections, Appl. Sci.-Basel, 8, 10.3390/app8040627, 2018.

Yi, Y., Zhang, Z., Zhang, W., Xu, Q., Deng, C., and Li, Q.: GIS-based earthquake-triggered-landslide susceptibility mapping with an integrated weighted index model in Jiuzhaigou region of Sichuan Province, China, Natural Hazards and Earth System

705   Sciences, 19, 1973-1988, 10.5194/nhess-19-1973-2019, 2019.

Traffic accident article (case2): https://www.mk.co.kr/news/society/view/2021/12/1113889/, last access: April 27, 2022.

Zerr, R. J.: Freezing rain: An observational and theoretical study, Journal of Applied Meteorology, 36, 1647-1661, 1997.